BNL-229021-2025-JAAM

GRP-COAP-84

# Elucidation of Marcus Relationships for Hydride Transfer Reactions Involving Transition Metal Hydrides

A. Kumar, M. Z. Ertem

To be published in "Journal of the American Chemical Society"

August 2025

Chemistry Department

**Brookhaven National Laboratory**

**U.S. Department of Energy**

USDOE Office of Science (SC), Basic Energy Sciences (BES). Chemical Sciences, Geosciences & Biosciences Division (CSGB)

# DISCLAIMER

# Elucidation of Marcus Relationships for Hydride Transfer Reactions Involving Transition Metal Hydrides

Abhishek Kumar,[a] Mehmed Z. Ertem,[b,*] Nilay Hazari,[a,*] & Alexander J. M. Miller[c,*]

[a]Department of Chemistry, Yale University, P. O. Box 208107, New Haven, Connecticut, 06520, USA. E-mail: nilay.hazari@yale.edu

[b]Chemistry Division, Brookhaven National Laboratory, Upton, New York 11973, USA. E-mail: mzertem@bnl.gov

[c]Department of Chemistry, University of North Carolina at Chapel Hill, Chapel Hill, North Carolina 27599, USA. E-mail: ajmm@email.unc.edu

## Abstract

The rate of hydride transfer from three Ir hydride complexes of the type Cp*Ir($^{R}$bpy)H$^{+}$ (Cp* = $C_5Me_5$; $^{R}$bpy = 4,4'-R-2,2'-bipyridine, R = OMe, H, $CO_2Me$,) to six N-methylacridinium ($^{R}$Acr$^{+}$) acceptors with electronically different substituents in the 2- and 2,7-positions were measured. Using the thermodynamic hydricity of the donors and the hydride affinity of the acceptors the thermodynamic driving forces for hydride transfer were determined. Brønsted plots, which correlate kinetic and thermodynamic hydricity, demonstrate distinct linear free energy relationships for each complex, with different Brønsted α values. Thus, at the same driving force hydride transfer from Cp*Ir($^{OMe}$bpy)H$^{+}$ is faster than for Cp*Ir(bpy)H$^{+}$ or Cp*Ir($^{CO2Me}$bpy)H$^{+}$. Experimental and computational analyses are consistent with a concerted hydride transfer mechanism for all Ir complexes. As the thermodynamic driving force increases an earlier transition state is observed and all transition states also include π-stacking interactions between the donor and acceptor, which likely contribute to the different α values. The experimental data fits well to the Marcus model, enabling the determination of reorganization energies ($\lambda$) that range from 58-69 kcal mol$^{-1}$. These are lower than $\lambda$ values for hydride transfer reactions involving organic donors and acceptors. This work provides a rare example of the correlation of kinetic and thermodynamic hydricity using only experimental data and shows that hydride transfer reactions involving metal hydrides can follow Marcus theory. The findings offer insight into controlling metal-catalyzed hydride transfer reactions, which is valuable for designing improved systems for a range of transformations.

## Introduction

Transition metal hydrides are key intermediates in a range of important catalytic transformations[1] that have applications for the synthesis of fine and commodity chemicals,[2] pharmaceuticals,[3,4] monomers for polymerization,[5] and molecules for energy storage.[6] The transfer of a metal hydride to an organic substrate (Eq 1) is the turnover-limiting step in many of these processes. Thus, developing fundamental understanding of this elementary process is expected to aid the design of improved systems. Knowledge about hydride transfer from a metal complex is also anticipated to benefit transformations that involve the microscopic reverse process, the transfer of a hydride from an organic substrate to generate a metal hydride, which is the turnover-limiting step in many dehydrogenation reactions.[7]

$$L_nM{-}H + \text{substrate} \rightleftharpoons L_nM^+ + H\text{-substrate}^- \quad \text{(Eq 1)}$$

Substrates include: $CO_2$, olefins, ketones, N-heterocycles *etc.*

Many studies exploring hydride transfer reactions have focused on determining and understanding thermodynamic hydricity ($\Delta G°_{H-}$), which is the free energy required for heterolytic cleavage of a transition metal hydride bond (M–H) to generate a $H^-$ ion in solution.[8] Thermodynamic hydricity is an effective tool for predicting the driving force of a hydride transfer reaction. Emphasis has also been placed on measuring kinetic hydricity, which is the elementary rate constant for a hydride transfer reaction (and is connected to the free energy of activation, $\Delta G^{‡}_{H-}$).[8b,8e] Kinetic hydricity is important for predicting rates and often selectivity in catalysis when hydride transfer is the turnover limiting step.

Linear free energy relationships (LFERs), which correlate thermodynamic and kinetic parameters, have found extensive use in designing improved catalysts and understanding elementary processes.[9] Marcus theory, which is commonly used to model the kinetics and thermodynamics of electron,[10] hydrogen atom,[11] and group transfer[12] reactions is one of the most powerful tools to understand LFERs. Apart from enabling predictions about the rates of reactions, it has provided unprecedented insight into the nature of transition states,[13] the synchronicity of reactions,[14] and the effect of solvent on reaction barriers.[15]

Marcus theory can also be used to analyze LFERs for hydride transfer reactions between organic hydride donors and acceptors.[16] For example, Kreevoy and co-workers used Brønsted plots, which relate thermodynamic driving force (equilibrium constant) and rate constant, to demonstrate that organic hydride transfer reactions followed a Marcus relationship.[16a,16c-e] In reactions involving thirty-five structurally similar hydride donors and acceptors based on pyridiniums, quiniliniums, acridiniums, and phenanthridiniums, they concluded that over a

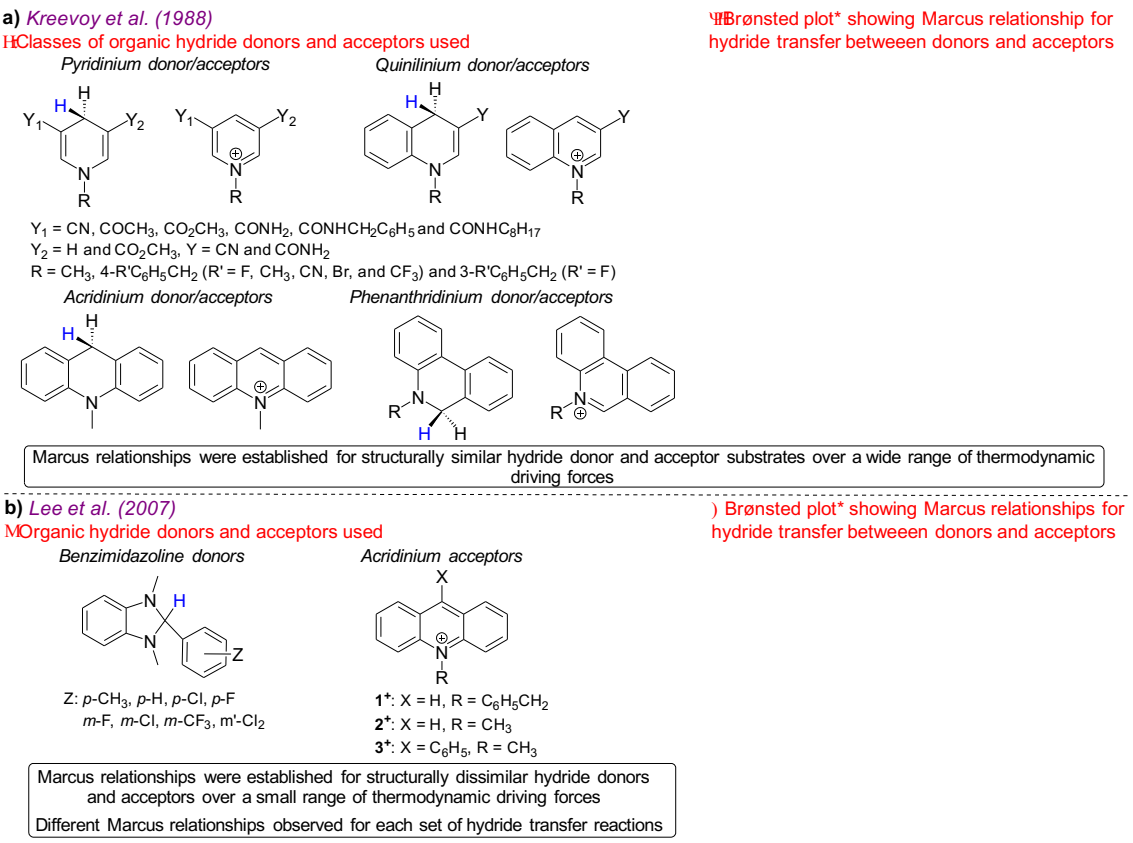


**Figure 1:** Selected previous examples of LFERs demonstrating that hydride transfer reactions between organic hydride donors and acceptors can be analyzed using Marcus theory. **a)** Kreevoy *et al.*'s work showing a single Marcus relationship for different donors and acceptors, and **b)** Lee *et al.*'s work showing different Marcus relationships depending on the structure of the acceptor. *In the Brønsted plots $k_1$ is the elementary rate constant for hydride transfer and $K_{eq}$ is the equilibrium constant for the hydride transfer reaction.

range of 26 ln $K_{eq}$ units the rates of hydride transfer followed a single Marcus relationship. Brønsted α values of 0.37-0.47 and reorganization energies (λ) of 88-98 kcal mol$^{-1}$ (Figure 1a) were determined in a highly polar 2-propanol and water (4:1, v/v) solvent mixture.[16c] This work implies that, for the molecules studied, the rates of hydride transfer can be predicted based only on the driving force and the exact structures of the donor and acceptor are unimportant. In related work using benzimidazoline hydride donors and acridinium hydride acceptors, Lee *et al*. observed three different parallel Marcus correlations rather than a single relationship depending on the nature of the acceptor (Figure 1b). The λ values ranged from 84.3-120.0 kcal mol$^{-1}$ in 2-propanol and water (4:1, v/v).[16f] Lee's results indicate that the structure of the hydride acceptor can impact the relationship between the rate and thermodynamic driving force, but the reasons why variations in the structures caused different relationships were not elucidated.

In recent work, Glusac and co-workers used Marcus theory to analyze hydride transfer reactions between organic hydride donors, such as substituted 2,3-dihydrobenzimidazoles, and

$CO_2$.[17] They proposed that the λ values associated with these reactions (~70-74 kcal $mol^{-1}$ in DMSO) would lead to prohibitively slow rates of hydride transfer in organocatalytic $CO_2$ reduction. It was postulated the large self-exchange reorganization energies associated with the 2,3-dihydrobenzimidazoles caused the slow rates of hydride transfer and that systems with lower self-exchange reorganization energies were required. Metal hydrides were identified as donors that may have lower self-exchange reorganization energies.[17-18] However, experimental information on λ values for hydride transfer from metal complexes is limited. Further, directly connecting LFERs from organic hydrides to transition metal hydrides is complicated because they are often larger and there are more variations in electronic structure and mechanistic pathways. For example, metal hydrides are more likely to participate in redox chemistry and proceed via stepwise mechanisms involving electron transfer (ET) followed by hydrogen atom transfer (HAT).[19] Thus, explicit studies of Marcus parameters of hydride transfer reactions from metal hydrides are necessary.

To date, there are a limited number of studies of hydride transfer reactions from metal complexes that correlate the rate of hydride transfer with the thermodynamic hydricity of the metal hydride to generate a LFER.[20] These studies typically cannot be used to assess if hydride transfer reactions follow Marcus theory due to limitations in the experimental data. For example, we showed that in reactions between ($^{R}$bpy)$Re(CO)_3H$ ($^{R}$bpy = 4,4'-R-2,2'-bipyridine; R = OMe, $^{t}$Bu, Me, H, Br, COOMe, $CF_3$) and 5 different hydride acceptors, the reactions were sensitive to the steric properties of the acceptor (Figure 2a).[20e] This prevented accurate analysis of the data using Marcus theory. Recently, Dixon, Wiedner *et al*. showed that $\Delta G^{\ddagger}$ for the cross-reaction between $HRh(dmpe)_2$ and $Ar_2CO$ acceptors (determined based on catalytic turnover frequencies) can be predicted from experimentally measured values of $\Delta G^{\ddagger}$ for the $H^-$ self-exchange reactions between $HRh(dmpe)_2$/$[Rh(dmpe)_2]^+$ and $[Ar_2CHO]^-$/$Ar_2CO$ (Figure 2b).[21] This was the first example of the Marcus cross-relation being used for hydride transfer reactions involving a metal hydride and a λ value of ~80.0 kcal $mol^{-1}$ was estimated. Nevertheless, to our knowledge there are no stoichiometric studies that directly measure the elementary rate constant for hydride transfer in a manner which allows modelling using Marcus theory. Further, to assess the feasibility and limitations of the Marcus model for analyzing hydride transfer reactions there is a need for more data across a range of driving forces.

In this work, we experimentally measure the rates of hydride transfer from three Ir complexes of the form $Cp^*Ir(^{R}bpy)H^+$ ($Cp^* = C_5Me_5$; R = OMe, H, $CO_2Me$) to six 2- or 2,7-substituted

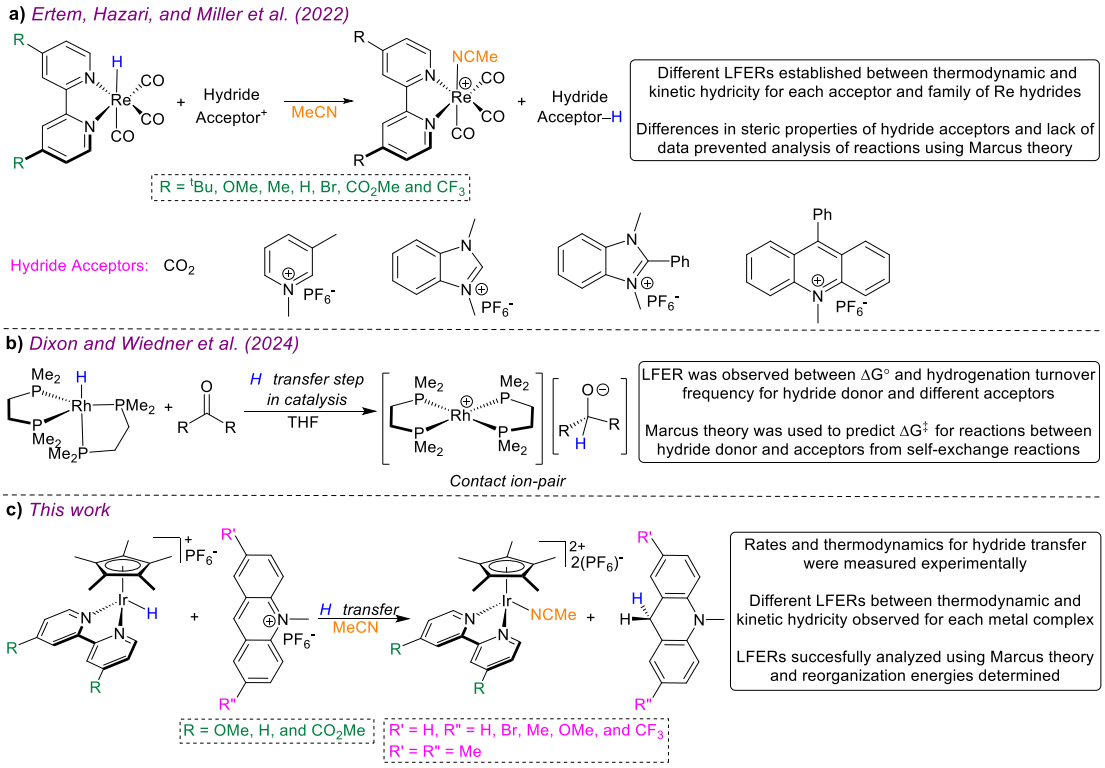


**Figure 2:** Selected previous examples of LFERs between metal hydride donors and organic acceptors: **a)** Our work showing a correlation between thermodynamic and kinetic hydricity. **b)** Dixon and Wiedner's work showing that catalytic turnover frequency (TOF) in ketone hydrogenation correlates with thermodynamic hydricity and the TOF can be predicted using the Marcus cross-relation involving calculating self-exchange rates. **c)** Summary of this work which develops LFERs for $H^-$ transfer reactions between sterically similar but electronically diverse metal hydrides of type Cp*Ir($^{R}$bpy)$H^+$ and $^{R}Acr^+$ acceptors. Each metal complex gives a different LFER that can be independently modelled using Marcus theory.

acridinium salt acceptors. This enabled us to determine the rates of hydride transfer across a driving force of approximately 10 kcal mol$^{-1}$ (ln $K_{eq}$ = ~ 7-22) without significantly altering the steric properties of the substrates. Experimental and computational studies provide evidence for a direct hydride transfer pathway instead of stepwise pathways involving initial proton transfer (PT), ET, or HAT. Brønsted plots reveal that hydride transfers from the three Ir complexes follow different LFERs with Cp*Ir(bpy)$H^+$ and Cp*Ir($^{CO2Me}$bpy)$H^+$ giving slower rates and similar α values (~0.5), while Cp*Ir($^{OMe}$bpy)$H^+$ gives faster rates and a lower α value (~0.3). The LFERs for each complex fit well to a Marcus model, which enables us to determine λ values ranging from 58-69 kcal mol$^{-1}$ for these reactions. The presence of subtle interactions such as π-stacking between the donor and acceptor in the transition state structures for hydride transfer is likely partially responsible for the differences in α and λ. Overall, our results provide one of the first demonstrations that Marcus theory can be used to model hydride transfer reactions involving metal hydrides, but suggest that subtle structural variations influence reaction rates. The fundamental information in this work provides guidelines on how to modulate the rates of hydride transfer reactions, which is likely relevant to catalysis.

## Results

*Selection, Synthesis, and Characterization of Hydride Donors and Acceptors*

We selected the known Ir hydrides, Cp*Ir($^{R}$bpy)H$^{+}$ (R = OMe, H, COOMe), as our hydride donors because it has been demonstrated that they participate in hydride transfer reactions[22] and there is a significant change of 2.5 kcal mol$^{-1}$ in the thermodynamic hydricity of the complexes as the substituents in the 4 and 4'-positions of the bpy ligand are varied (Table 1). Further, the changes in thermodynamic hydricity that occur with different substituents in the 4 and 4'-positions of the bpy ligand are not expected to interfere with the steric properties around the Ir center. Cp*Ir($^{OMe}$bpy)H$^{+}$ and Cp*Ir(bpy)H$^{+}$ were synthesized following literature procedures,[22d,23] while Cp*Ir($^{CO2Me}$bpy)H$^{+}$ was prepared using a new route (Scheme S1). In all cases the complexes were prepared with $PF_6^-$ as the anion, because of its weakly coordinating nature.[24]

**Table 1:** Thermodynamic hydricities (in MeCN) of hydride donors and hydride affinities (the thermodynamic hydricity of the conjugate hydride donor) of hydride acceptors used in this work.

**Hydride Donors**

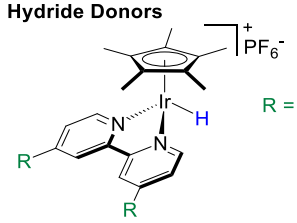


R = OMe (Cp*Ir($^{OMe}$bpy)H$^{+}$)
H (Cp*Ir(bpy)H$^{+}$)
$CO_2Me$ (Cp*Ir($^{CO2Me}$bpy)H$^{+}$)

**Hydride Acceptors**

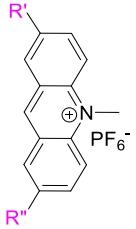


R' = H, R" = OMe ($^{OMe}$Acr$^{+}$)
R' = H, R" = Me ($^{Me}$Acr$^{+}$)
R' = H, R" = H (Acr$^{+}$)
R' = H, R" = Br ($^{Br}$Acr$^{+}$)
R' = H, R" = $CF_3$ ($^{CF3}$Acr$^{+}$)
R' = R" = Me ($^{(Me)2}$Acr$^{+}$)

| Hydride Donors | Thermodynamic Hydricity ($\Delta G_{H^-}$ in kcal mol$^{-1}$)[a] |
|---|---|
| Cp*Ir($^{OMe}$bpy)H$^{+}$ | 61.1 |
| Cp*Ir($^{H}$bpy)H$^{+}$ | 62.0 |
| Cp*Ir($^{CO2Me}$bpy)H$^{+}$ | 63.6 |

| Hydride Acceptors | Hydride Affinity ($\Delta G_{H^-}$ in kcal mol$^{-1}$)[a] |
|---|---|
| $^{(Me)2}$Acr$^{+}$ | 67.5 |
| $^{OMe}$Acr$^{+}$ | 68.2 |
| $^{Me}$Acr$^{+}$ | 68.8 |
| Acr$^{+}$ | 70.0 |
| $^{Br}$Acr$^{+}$ | 72.3 |
| $^{CF3}$Acr$^{+}$ | 74.4 |

[a]The error on thermodynamic hydricity and affinity values is estimated to be ±1 kcal mol$^{-1}$.

The weakest hydride donor in our series is Cp*Ir($^{CO2Me}$bpy)H$^{+}$ with a thermodynamic hydricity of 63.6 kcal mol$^{-1}$ in acetonitrile (MeCN).[22d] Thus, to ensure that hydride transfer reactions from all our Cp*Ir($^{R}$bpy)H$^{+}$ complexes were thermodynamically favorable, we needed to use a family of hydride acceptors with hydride affinities greater than 63.6 kcal mol$^{-1}$ in MeCN. (The hydride affinity is the thermodynamic hydricity of the conjugate hydride donor.) Previously, it was reported that N-methylacridinium (Acr$^{+}$) has a hydride affinity of 70.0 kcal mol$^{-1}$.[8c] Therefore, hydride transfer from Cp*Ir($^{CO2Me}$bpy)H$^{+}$ to Acr$^{+}$ is estimated to be 6.4 kcal mol$^{-1}$ downhill in MeCN. Apart from meeting our thermodynamic requirement, Acr$^{+}$ is an attractive

hydride acceptor because both it and its conjugate hydride donor, N-methylacridine (AcrH), have been utilized extensively in organic hydride transfer reactions.[16a,16c,16i] Further, we hypothesized that we could generate a family of N-methylacridiniums with different hydride affinities, without significant variation in steric profile, by adding substituents in the 2 and/or 7-positions of $Acr^+$. Using modified literature procedures[25] we synthesized a family of 2-substituted N-methylacridiniums ($^{R}Acr^+$; R = $CF_3$, Br, Me, or OMe) as $PF_6$ salts and a N-methylacridinium with methyl substituents in the 2 and 7-positions ($^{(Me)2}Acr^+$) (Scheme S2). We also synthesized the corresponding N-methylacridines ($^{R}AcrH$, see Section SII in the SI), which are the expected products of hydride transfer to $^{R}Acr^+$.

To determine the hydride affinities of our series of substituted $^{R}Acr^+$ acceptors, we used equilibrium exchange measurements. Specifically, starting with unsubstituted $Acr^+$, which has a known thermodynamic hydricity as a benchmark,[8c] we measured the equilibrium constant for hydride transfer when AcrH was treated with a substituted $^{R}Acr^+$ in MeCN (see Figure 3 for a generic representation of the equilibrium exchange reaction). Using the value of the equilibrium constant determined by NMR spectroscopy and the known thermodynamic hydricity of AcrH, the hydride affinity of the $^{R}Acr^+$ could be determined (see Section SIII).

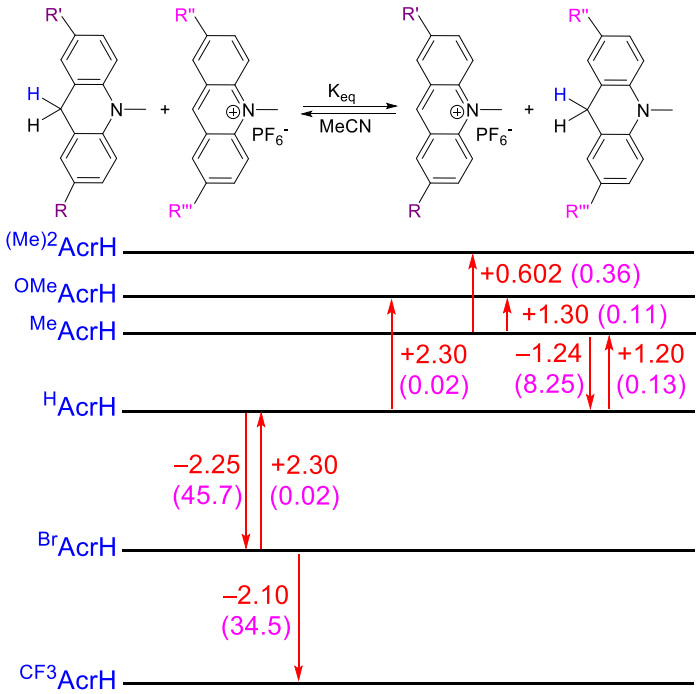


**Figure 3:** Experimentally determined relative free energies (in red) for hydride transfer between different $^{R}Acr^+$ acceptors and $^{R}AcrH$ donors in MeCN. The free energies were determined from the equilibrium constants, which were measured using NMR spectroscopy and are shown in pink in parentheses. Vertical arrows show the direction of established equilibria. The errors on the values are estimated to be ±1 kcal $mol^{-1}$. Given that unsubstituted AcrH has a known thermodynamic hydricity it was possible to use these relative free energies to determine the thermodynamic hydricity of all substituted acridines ($^{R}AcrH$) studied in this work (see Table 1).

Once the hydride affinity of a new $^{R}Acr^{+}$ was established, it could be used to determine the thermodynamic hydricity of a $^{R}AcrH$ with different substituents. Figure 3 shows the equilibrium constants and corresponding relative free energies for hydride exchange measured for our series of $^{R}Acr^{+}$ acceptors. In some cases, equilibrium constants were measured in both directions to ensure accurate values. The hydride affinities for our full series of $^{R}Acr^{+}$ range from 67.5 kcal mol$^{-1}$ for $^{(Me)2}Acr^{+}$ to 74.4 kcal mol$^{-1}$ for $^{CF3}Acr^{+}$ (Table 1). This indicates that hydride transfer to more electron deficient $^{CF3}Acr^{+}$ will be more thermodynamically favorable than to electron rich $^{(Me)2}Acr^{+}$. Combining our Ir hydride donors with our acridinium hydride acceptors the range of driving forces for hydride transfer is between 3.9 and 13.3 kcal mol$^{-1}$. Hence, our series of compounds provides a variety of driving forces for hydride transfer, while maintaining a similar steric profile.

*Experimental Measurements of Hydride Transfer Rates and Correlation Between Kinetic and Thermodynamic Hydricity*

Initial experiments between complexes of the type Cp*Ir($^{R}$bpy)H$^{+}$ and the unsubstituted acceptor Acr$^{+}$ in MeCN showed that hydride transfer to form Cp*Ir($^{R}$bpy)(MeCN)$^{2+}$ and AcrH was quantitative and rapid. Due to the fast rates of these reactions, we elucidated the kinetics of hydride transfer using a stopped-flow instrument with a UV-Vis detector. As expected, the reactions are first-order in [Cp*Ir($^{R}$bpy)H$^{+}$] and [Acr$^{+}$] giving an overall rate law of $k_1$[Cp*Ir($^{R}$bpy)H$^{+}$][Acr$^{+}$] (Figures S40-S45). The rate constants follow the thermodynamic favorability of the reactions. Hydride transfer from the electron-rich hydride, Cp*Ir($^{OMe}$bpy)H$^{+}$,

**Table 2:** Rate constants for hydride transfer from Cp*Ir($^{R}$bpy)H$^{+}$ (R = OMe, H, and $CO_2Me$) and $^{R}Acr^{+}$ acceptors (R = $Me_2$, OMe, Me, H, Br and $CF_3$) in MeCN at 303 K under $N_2$.

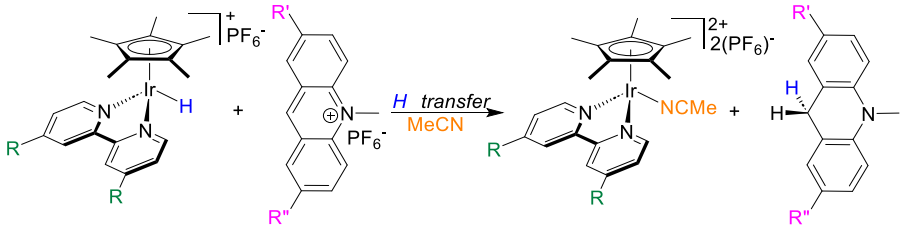


| $^{R}Acr^{+}$ | $k_1$ ($M^{-1}s^{-1}$)[a] | | |
|---|---|---|---|
| **R =** | **Cp*Ir($^{OMe}$bpy)H$^{+}$** | **Cp*Ir(bpy)H$^{+}$** | **Cp*Ir($^{CO2Me}$bpy)H$^{+}$** |
| $CF_3$ | 1.3 x $10^6$ | 1.2 x $10^5$ | 1.4 x $10^4$ |
| Br | 8.5 x $10^5$ | 6.1 x $10^4$ | 3.8 x $10^3$ |
| H | 1.4 x $10^5$ | 7.1 x $10^3$ | 2.2 x $10^2$ |
| Me | 8.7 x $10^4$ | 2.2 x $10^3$ | 6.7 x $10^1$ |
| $(Me)_2$ | 5.8 x $10^4$ | 6.2 x $10^2$ | 4.7 x $10^1$ |
| OMe | 3.6 x $10^4$ | 5.8 x $10^2$ | Not determined[b] |

[a]The errors associated with the $k_1$ values are ±5%.[b]We were unable to experimentally determine the rate of hydride transfer from Cp*Ir($^{CO2Me}$bpy)H$^{+}$ to $^{OMe}Acr^{+}$ because the rate was so slow that side decomposition reactions occurred.

which is the most thermodynamically favorable reaction ($\Delta G = -8.9$ kcal mol$^{-1}$), was significantly faster than from the unsubstituted hydride, Cp*Ir(bpy)H$^+$ ($\Delta G = -8.0$ kcal mol$^{-1}$), which in turn gave a faster rate than the electron withdrawing hydride Cp*Ir($^{CO2Me}$bpy)H$^+$ ($\Delta G = -6.4$ kcal mol$^{-1}$) (Table 2). The large differences in rates (three orders of magnitude) as the electronic properties of the metal hydride are changed are consistent with previous observations in the literature for hydride transfer reactions.[20b,20e,26]

To gain further insight into the hydride transfer reactions, the activation parameters for hydride transfer from Cp*Ir($^{R}$bpy)H$^+$ to Acr$^+$ were determined using Eyring analysis (Figures S46-S48 and Table 3). Consistent with a second-order reaction in which two molecules are combining to form one molecule in the transition state, the entropies of activation are large and negative. The activation entropies are not all the same, however, with the activation entropy for hydride transfer from Cp*Ir($^{OMe}$bpy)H$^+$ surprisingly being almost 10 cal mol$^{-1}$ K$^{-1}$ less negative compared to Cp*Ir(bpy)H$^+$ or Cp*Ir($^{CO2Me}$bpy)H$^+$. The activation enthalpy for Cp*Ir($^{OMe}$bpy)H$^+$ is similar to that for Cp*Ir(bpy)H$^+$ (3.4 kcal mol$^{-1}$), but both are lower than for Cp*Ir($^{CO2Me}$bpy)H$^+$ (4.7 kcal mol$^{-1}$).

**Table 3:** Activation parameters for hydride transfer from Cp*Ir($^{R}$bpy)H$^+$ (R = OMe, H, and $CO_2Me$) to the unsubstituted acceptor, Acr$^+$, in MeCN at 303 K.

| Complex | $\Delta H^{\ddagger}$ (kcal mol$^{-1}$) | $\Delta S^{\ddagger}$ (cal mol$^{-1}$ K$^{-1}$) | $\Delta G^{\ddagger}_{303}$ (kcal mol$^{-1}$) |
|---|---|---|---|
| Cp*Ir($^{OMe}$bpy)H$^+$ | 3.5 ± 0.4 | -21.8 ± 2.1 | 10.2 ± 1.0 |
| Cp*Ir(bpy)H$^+$ | 3.4 ± 0.3 | -29.6 ± 2.9 | 12.4 ± 1.2 |
| Cp*Ir($^{CO2Me}$bpy)H$^+$ | 4.7 ± 0.5 | -31.7 ± 3.1 | 14.3 ± 1.4 |

[a]The errors associated with the $k_1$ values are ±5%.

To complement our experiments varying the electronic properties of the hydride donor, we next determined the kinetics of hydride transfer from Cp*Ir($^{R}$bpy)H$^+$ to our full series of hydride acceptors ($^{R}$Acr$^+$) with different electronic properties. For all three Ir complexes, the same trend was observed. Hydride transfer to more electron-deficient hydride acceptors, for example $^{CF3}$Acr$^+$, is significantly faster than hydride transfer to more electron-rich hydride acceptors, for example $^{(Me)2}$Acr$^+$ (Table 2). This follows expected trends based on the thermodynamic favorability of the hydride transfer reaction and suggests a correlation between kinetic and thermodynamic hydricity.

We constructed a Brønsted plot of ln($K_{eq}$) vs. ln($k_1$), where $K_{eq}$ is the equilibrium constant for hydride transfer derived from the experimental thermodynamic hydricity of the Ir hydrides and the hydride affinity of the acridinium acceptors and $k_1$ is the rate constant for hydride transfer at 303 K in MeCN (Figure 4a). For all three Ir complexes, a clear correlation was observed between the thermodynamic driving force and the rate of the reaction, but the correlation was

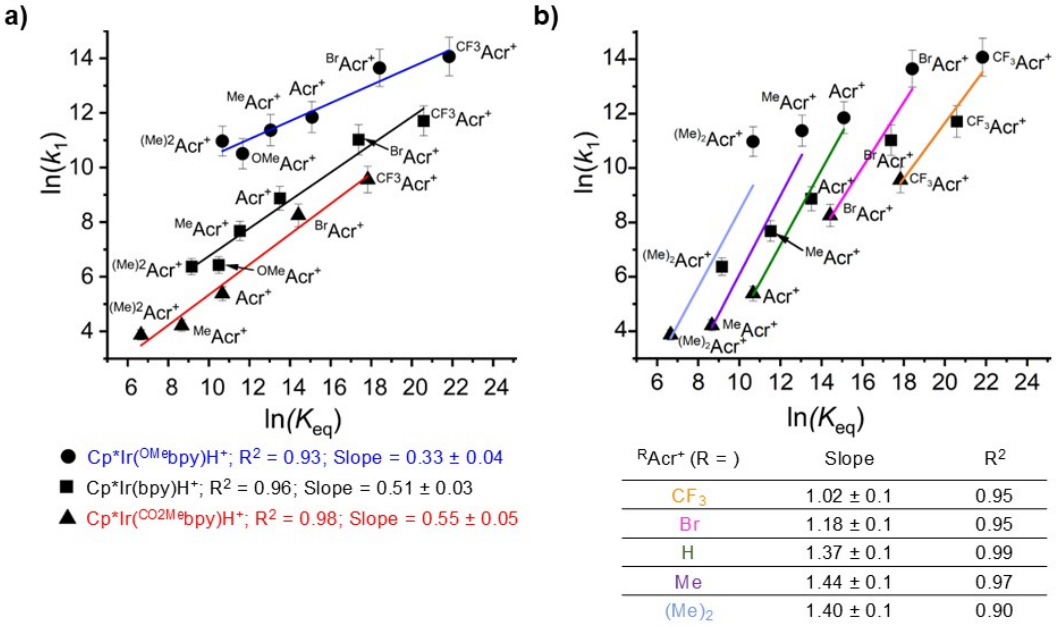


| $^{R}$Acr$^{+}$ (R = ) | Slope | $R^2$ |
|---|---|---|
| $CF_3$ | 1.02 ± 0.1 | 0.95 |
| Br | 1.18 ± 0.1 | 0.95 |
| H | 1.37 ± 0.1 | 0.99 |
| Me | 1.44 ± 0.1 | 0.97 |
| $(Me)_2$ | 1.40 ± 0.1 | 0.90 |

**Figure 4:** Brønsted plot for H$^-$ transfer from all three Cp*Ir($^{R}$bpy)H$^+$ (R = OMe, H, and $CO_2Me$) hydride donors to the series of acridinium acceptors $^{R}$Acr$^+$ (R = $(Me)_2$, OMe, Me, H, Br, and $CF_3$). **a)** Trendlines drawn for the three Ir hydride donors and **b)** trendlines drawn for the $^{R}$Acr$^+$ hydride acceptors. The same data is used in **a** and **b**. Reactions conditions: Cp*Ir($^{R}$bpy)H$^+$ = $^{R}$Acr$^+$ = 0.44 mM at 303 K in MeCN under $N_2$.

different for all three complexes. Thus, different reaction rates were observed for hydride transfer reactions at the same specific driving force for hydride transfer. For example, at a driving force of 7.2 kcal mol$^{-1}$ ($\ln(K_{eq}) = 12$) the rate of hydride transfer from Cp*Ir($^{OMe}$bpy)H$^+$ to Acr$^+$ was approximately 26 times faster than for hydride transfer from Cp*Ir(bpy)H$^+$ to $^{Me}$Acr$^+$. This indicates that thermodynamic driving force is not the only factor in determining the rate of hydride transfer and the structure of the Ir complex is important. The difference in rates as a function of driving force is smaller for Cp*Ir(bpy)H$^+$ compared to Cp*Ir($^{CO2Me}$bpy)H$^+$. At a driving force of 7.2 kcal mol$^{-1}$ ($\ln(K_{eq}) = 12$), Cp*Ir(bpy)H$^+$ only transfers a hydride ~4 times faster than Cp*Ir($^{CO2Me}$bpy)H$^+$. Further, there are differences in the slopes of the Brønsted plots between the three complexes. An $\alpha$ value of 0.33 was observed for Cp*Ir($^{OMe}$bpy)H$^+$, compared to values of 0.51 and 0.58 for Cp*Ir(bpy)H$^+$ and Cp*Ir($^{CO2Me}$bpy)H$^+$, respectively. Consequently, as the driving force increases, the difference in rates between Cp*Ir($^{OMe}$bpy)H$^+$, Cp*Ir(bpy)H$^+$ and Cp*Ir($^{CO2Me}$bpy)H$^+$ become smaller. One possible explanation for the differences in $\alpha$ values between Cp*Ir($^{OMe}$bpy)H$^+$ and Cp*Ir(bpy)H$^+$ and Cp*Ir($^{CO2Me}$bpy)H$^+$ is that the hydride transfer reaction proceeds via different mechanisms. The pathway for hydride transfer is explored further using a combination of experimental and theoretical methods in subsequent sections.

The data from Figure 4a is represented in a different manner in Figure 4b, where instead of

trendlines being included for each Ir complex, trendlines are shown for each acridinium ($^{R}Acr^{+}$) acceptor. Although each line only contains three points, which limits analysis, the linear correlations are relatively strong. Each $^{R}Acr^{+}$ acceptor gives a distinct correlation with the series of Ir complexes, indicating that the rate depends on the structure of the acceptor and not just the driving force of the reaction. At the same driving force more electron rich $^{R}Acr^{+}$ acceptors give faster rates of hydride transfer. Additionally, as the $^{R}Acr^{+}$ acceptor becomes less electron-deficient the slope of the correlation decreases markedly. Hence, for the most electron rich acceptor for which we have three data points, $^{(Me)2}Acr^{+}$, the slope is 1.40, whereas for the least electron rich acceptor, $^{CF3}Acr^{+}$, the slope is 1.02.

*Kinetic Isotope Effects Associated with Hydride Transfer*

Kinetic isotope effects (KIEs) provide valuable information about the mechanism of hydride transfer reactions.[20e,27] To search for any possible change in mechanism and analyze trends in driving force, we synthesized complexes of the type Cp*Ir($^{R}$bpy)D$^{+}$ (see Section SVIII) and measured the KIE ($k_H/k_D$) for hydride transfer to several different acridinium acceptors. Table 4 collects three sets of KIE measurements at three different driving forces. Within each set of measurements, each of the three Ir hydride complexes is paired with an appropriate organic acceptor to achieve the desired driving force. Two trends are apparent in Table 4: (i) although the KIE values are similar at a given driving force, the most hydridic Ir hydride complex Cp*Ir($^{OMe}$bpy)H$^{+}$ has a slightly larger KIE in all cases (*e.g.* 1.3 vs 0.82 vs. 0.92 for a driving force of ca. 6.3 kcal mol$^{-1}$, entries 1-3); (ii) the KIE values for all complexes increase as the driving force increases. However, the magnitude of the change in KIE as a function of driving

**Table 4:** Experimentally determined KIE values and thermodynamic driving forces for hydride transfer reaction between Cp*Ir($^{R}$bpy)H$^{+}$ (R = OMe, H, and $CO_2Me$) and selected $^{R}Acr^{+}$ acceptors (R = $Me_2$, Me, OMe, H, Br and $CF_3$) in MeCN at 303 K under $N_2$.

| Entry | Hydride donor | Hydride acceptor | Thermodynamic driving force (kcal mol$^{-1}$)[a] | KIE ($k_H/k_D$)[b] |
|---|---|---|---|---|
| 1 | Cp*Ir($^{CO2Me}$bpy)H$^{+}$ | $Acr^{+}$ | 6.4 | 0.92 |
| 2 | Cp*Ir(bpy)H$^{+}$ | $^{OMe}Acr^{+}$ | 6.2 | 0.82 |
| 3 | Cp*Ir($^{OMe}$bpy)H$^{+}$ | $^{(Me)2}Acr^{+}$ | 6.4 | 1.3 |
| 4 | Cp*Ir($^{CO2Me}$bpy)H$^{+}$ | $^{Br}Acr^{+}$ | 8.6 | 0.99 |
| 5 | Cp*Ir(bpy)H$^{+}$ | $Acr^{+}$ | 8 | 1.08 |
| 6 | Cp*Ir($^{OMe}$bpy)H$^{+}$ | $Acr^{+}$ | 8.8 | 1.7 |
| 7 | Cp*Ir($^{CO2Me}$bpy)H$^{+}$ | $^{CF3}Acr^{+}$ | 10.7 | 1.13 |
| 8 | Cp*Ir(bpy)H$^{+}$ | $^{Br}Acr^{+}$ | 10.2 | 1.74 |
| 9 | Cp*Ir($^{OMe}$bpy)H$^{+}$ | $^{Br}Acr^{+}$ | 11.4 | 2.1 |

[a]Determined by comparing the thermodynamic hydricity of the Ir complex with the hydride affinity of the acridinium acceptor. [b]The errors associated with the values are ±5%.

force varied significantly across the series of complexes. For Cp*Ir($^{CO2Me}$bpy)H$^+$, the KIE only increased by 0.21 as the driving force was increased, whereas for Cp*Ir(bpy)H$^+$, and Cp*Ir($^{OMe}$bpy)H$^+$, the KIEs increased by approximately 0.8.

*Elucidation of the Pathway for Hydride Transfer*

Hydride transfer can occur via a direct concerted mechanism, or via other pathways that involve initial ET, PT, or HAT (Figure 5). Although, it is hard to obtain direct experimental evidence for a concerted hydride transfer, it is possible to perform experiments that eliminate pathways involving initial ET or PT for hydride transfer. To investigate a pathway involving initial ET (Figure 5b), cyclic voltammograms of all the Cp*Ir($^{R}$bpy)H$^+$ donors and $^{R}$Acr$^+$ acceptors were recorded in MeCN using 0.1 M tetrabutylammonium hexafluorophosphate as an electrolyte (see Section SIX). The thermodynamic driving forces associated with electron transfer ($\Delta G°_{ET}$) from Cp*Ir($^{R}$bpy)H$^+$ to $^{R}$Acr$^+$ acceptors were calculated based on the potentials corresponding to oxidation of the hydride donor and reduction of the acridinium acceptors (as tabulated in Table S2).[28] The thermodynamic driving forces for electron transfer ($\Delta G°_{ET}$) ranged from 20.5 to 33.9 kcal mol$^{-1}$ which were similar to those obtained from calculations (see Table 5 for Acr$^+$ and Table S2 for other acceptors). Given that Eyring analysis indicated that the activation energies for hydride transfer to Acr$^+$ ranged from 10-14 kcal mol$^{-1}$ (*vide supra* and Table 5), an initial step involving ET can be ruled out as the experimentally observed barriers are lower than would be required for a barrierless ET process (20.5 kcal mol$^{-1}$).

**a)** *Direct concerted hydride transfer*

$$Cp^*Ir(^{R}bpy)H^+ + {}^{R}Acr^+ \xrightarrow{HT} [Cp^*Ir(^{R}bpy)^+\text{----}H\text{----}{}^{R}Acr^+]^{\ddagger} \xrightarrow[MeCN]{} Cp^*Ir(^{R}bpy)(MeCN)^{2+} + {}^{R}AcrH$$

**b)** *Initial ET followed by subsequent PT ET or HAT*

$$Cp^*Ir(^{R}bpy)H^+ + {}^{R}Acr^+ \xrightarrow{ET} Cp^*Ir(^{R}bpy)H^{2+} + {}^{R}Acr^{\bullet} \xrightarrow[MeCN]{PT\ ET\ or\ HAT} Cp^*Ir(^{R}bpy)(MeCN)^{2+} + {}^{R}AcrH$$

**c)** *Initial PT followed by successive ET ET*

$$Cp^*Ir(^{R}bpy)H^+ + {}^{R}Acr^+ \xrightarrow{PT} Cp^*Ir(^{R}bpy) + {}^{R}AcrH^{2+} \xrightarrow[MeCN]{ET\ ET} Cp^*Ir(^{R}bpy)(MeCN)^{2+} + {}^{R}AcrH$$

**d)** *Initial HAT followed by ET*

$$Cp^*Ir(^{R}bpy)H^+ + {}^{R}Acr^+ \xrightarrow{HAT} Cp^*Ir(^{R}bpy)^+ + {}^{R}AcrH^+ \xrightarrow[MeCN]{ET} Cp^*Ir(^{R}bpy)(MeCN)^{2+} + {}^{R}AcrH$$

**Figure 5:** Possible pathways for hydride transfer from Cp*Ir($^{R}$bpy)H$^+$ to $^{R}$Acr$^+$ acceptors.

Next, we investigated the possibility of pathways involving initial PT from Cp*Ir($^{R}$bpy)H$^+$ to Acr$^+$ (Figure 5c). Previously, Miller and co-workers determined that complexes of the type Cp*Ir($^{R}$bpy)H$^+$ have p$K_a$ values between 16-24 in MeCN.[22d] We determined that the p$K_a$ of the conjugate acid of the unsubstituted acridinium acceptor (Acr$^+$) is less than <1.8 in MeCN (see Section SIX). Based on these p$K_a$ values, the free energies for PT ($\Delta G°_{PT}$) from the Ir hydrides

to the acridinium acceptor were determined to be significantly uphill ($\Delta G°_{PT} \geq 19.7$ kcal mol$^{-1}$, see Table 5). Given the activation energies for the overall hydride transfer are lower than 19.7 kcal mol$^{-1}$, pathways involving initial PT can be ruled out, consistent with the computationally determined free energy change values for PT (Table 5 and Tables S3-S4).

**Table 5:** Experimentally and computationally determined free energies ($\Delta G^{‡}$ and $\Delta G°$) for different elementary steps associated with hydride transfer from Cp*Ir($^{R}$bpy)H$^{+}$ to Acr$^{+}$. The values presented in parentheses are computationally determined using the MN15/def2-TZVP level of theory with the SMD continuum solvation model for MeCN.

| Hydride donors | $\Delta G^{‡}_{HT}$ (kcal mol$^{-1}$) | $\Delta G°_{ET}$ (kcal mol$^{-1}$) | $\Delta G°_{PT}$ (kcal mol$^{-1}$) | $\Delta G°_{HAT}$ (kcal mol$^{-1}$) |
|---|---|---|---|---|
| Cp*Ir($^{OMe}$bpy)H$^{+}$ | 10.2 ± 1.0 (11.6) | 24.6 (28.5) | ≥ 34.6 (80.9) | (27.0) |
| Cp*Ir(bpy)H$^{+}$ | 12.4 ± 1.2 (11.7) | 27.7 (30.2) | ≥ 29.7 (73.1) | (25.7) |
| Cp*Ir($^{CO2Me}$bpy)H$^{+}$ | 14.3 ± 1.4 (13.3) | 32.1 (32.4) | ≥ 19.7 (62.7) | (22.8) |

A pathway involving initial HAT from Cp*Ir($^{R}$bpy)H$^{+}$ would result in the formation of Cp*Ir($^{R}$bpy)$^{+}$ (Figure 5d). In principle, if we could experimentally determine the bond dissociation free energy (BDFE) of the Ir−H bond in Cp*Ir($^{R}$bpy)H$^{+}$, we could eliminate this pathway if the BDFE was greater than the activation energy for hydride transfer. Unfortunately, due to the instability of Cp*Ir($^{R}$bpy)$^{+}$, we were unable to determine BDFEs experimentally. Therefore, we used theoretical calculations to estimate the thermodynamics associated with an HAT pathway. To ensure the accuracy of our calculations, three different computational approaches were utilized. Here, we present the results from calculations at the MN15/def2-TZVP level with the SMD continuum solvation model for MeCN following geometry optimizations at the B3LYP-D3BJ level of theory in vacuum unless noted otherwise (see Section SXV). The calculations demonstrate that initial HAT ($\Delta G°_{HAT}$) is thermodynamically uphill by values ranging from 22.8 to 27.0 kcal mol$^{-1}$ (see Table 5 for results with Acr$^{+}$ and Table S5 for results with other acceptors), again suggesting that this is not a valid pathway for the hydride transfer reactions because even a barrierless HAT reaction would incur a higher activation energy than was experimentally observed.

The elimination of pathways involving initial PT, ET, or HAT, suggests that the hydride transfer reactions from Cp*Ir($^{R}$bpy)H$^{+}$ to $^{R}$Acr$^{+}$ are proceeding via direct hydride transfer. Therefore, we initially calculated the transition state structures and energies for direct hydride transfer from Cp*Ir($^{R}$bpy)H$^{+}$ to Acr$^{+}$ (Table 5). Good agreement was observed between the calculated and experimental activation energies, providing further support to the hypothesis that these reactions proceed via a single concerted step. The structures of the transitions state are shown in Figure 6, with selected geometrical parameters listed in Table 6. In all cases there is a clear interaction between the Ir hydride and the hydridophilic carbon center of the Acr$^{+}$ acceptor in

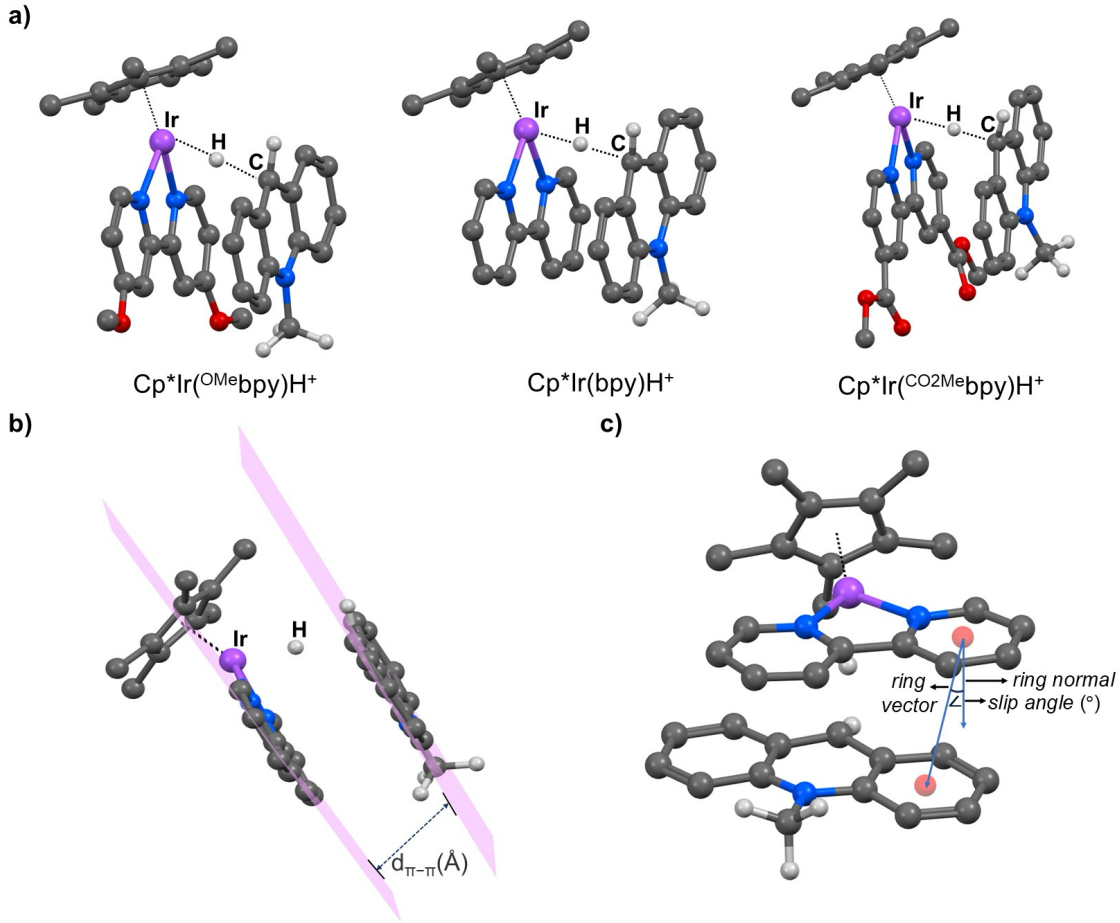


**Figure 6: a)** Calculated transition state structures for direct hydride transfer from Cp*Ir($^{R}$bpy)H$^{+}$ to Acr$^{+}$. The structures clearly show the interaction between the Ir center, the hydride and the hydridophilic carbon of Acr$^{+}$. **b)** Image showing the π–π stacking in the transition state for hydride transfer from Cp*Ir(bpy)H$^{+}$ to Acr$^{+}$. **c)** Schematic showing the offset, defined as the slip angle, between the aromatic rings involved in π–π stacking.

the transition state. The Ir−H bond distance in the transition state (1.713-1.761 Å) is elongated relative to the Ir−H bond distance in Cp*Ir($^{R}$bpy)H$^{+}$ (1.600-1.602 Å). One apparent trend is a shorter Ir–H distance in the transition state structure for stronger hydride donors. For example, the Ir−H bond distance in Cp*Ir($^{OMe}$bpy)H$^{+}$, 1.713 Å, is slightly shorter than the distance in Cp*Ir(bpy)H$^{+}$, 1.733 Å, which is in turn shorter than the distance in Cp*Ir($^{CO2Me}$bpy)H, 1.761 Å. There are even larger differences in the distances between the Ir−H and the incoming carbon atom of Acr$^{+}$, which reflects the degree of formation of the new $C_{Acr}$–H bond. For Cp*Ir($^{OMe}$bpy)H$^{+}$, the distance, 1.497 Å, is longer than for Cp*Ir(bpy)H$^{+}$, 1.430 Å, and Cp*Ir($^{CO2Me}$bpy)H, 1.406 Å.

To gain more insight into the nature of the transition states, we used the Intrinsic Bond Strength Index (IBSI)[29] to evaluate the percentage of bond cleavage of the Ir−H bond and bond formation of the $C_{Acr}$−H bond in the transition state for a reaction between Cp*Ir($^{R}$bpy)H$^{+}$ and

$Acr^+$ (Table 6). The data clearly shows that there is less Ir−H bond cleavage and less $C_{Acr}$−H bond formation for Cp*Ir($^{OMe}$bpy)$H^+$ and more Ir−H bond cleavage and more $C_{Acr}$−H bond formation for Cp*Ir($^{CO2Me}$bpy)$H^+$. This indicates a later transition state for hydride transfer from Cp*Ir($^{CO2Me}$bpy)$H^+$ with a stronger interaction between the hydride and hydridophilic carbon of $Acr^+$ ($C_{Acr}$), consistent with the observed Ir−H and $C_{Acr}$−H bond distances in the transition state. For all $^{R}Acr^+$ acceptors, theoretical calculations indicate an earlier transition state, as measured by Ir−H bond distances and the IBSI, for more thermodynamically favored reactions (Table S19).

**Table 6:** Geometrical parameters of calculated transition state structures for direct hydride transfer from Cp*Ir($^{R}$bpy)$H^+$ to $Acr^+$.

| Hydride donor | Bond distances (Å) | | Intrinsic bond strength index (%)[a] | | $d_{\pi-\pi}$ (Å)[b] | Slip angle (°)[c] |
|---|---|---|---|---|---|---|
| | Ir−H | $C_{Acr}$−H | Ir−H | $C_{Acr}$−H | | |
| Cp*Ir($^{OMe}$bpy)$H^+$ | 1.663 | 1.639 | 20.7 | 42.3 | 3.251 | 21.39 |
| Cp*Ir(bpy)$H^+$ | 1.683 | 1.594 | 23.8 | 49.1 | 3.269 | 21.14 |
| Cp*Ir($^{CO2Me}$bpy)$H^+$ | 1.710 | 1.512 | 28.9 | 51.8 | 3.220 | 23.22 |

[a]Intrinsic bond strength index values are used to calculate the bond cleavage percentage of the Ir−H bond and bond formation percentage of the $C_{Acr}$−H bond in the transition state structure. [b]$d_{\pi-\pi}$ (Å) is the distance between the π−planes of bpy and $Acr^+$ in the transition state structure. [c]Slip angle (°) is the angle between the ring vector joining the centroids of two aromatic rings of bpy and $Acr^+$ and the ring normal to one of the aromatic rings of bpy (see Figure 6c).

A feature of the transition state structures for hydride transfer from Cp*Ir($^{R}$bpy)$H^+$ to $Acr^+$ is the presence of clear π–π stacking interactions between one of the aromatic rings of bpy in Cp*Ir($^{R}$bpy)$H^+$ and one of the aromatic rings in $Acr^+$ (Figure 6b). The average distance between the planes containing the bpy and $Acr^+$ aromatic systems ($d_{\pi-\pi}$) is ~3.25 Å, which is consistent with previous reports of π stacking (Table 6).[30] The distance between the rings is similar for all three hydride donors, with no trend based on the substituents. An attribute of the π–π stacking is that the centroids in the aromatic rings in bpy and $Acr^+$ do not align directly, which is similar to what has been observed in many other systems with π–π stacking.[30] The degree of the offset, defined as the slip angle, can be quantified by measuring the angle between the ring vector between the centroids of the two rings and the normal from the centroid of the one of the rings (Figure 6c). The slip angles for all three complexes are between 21-23° suggesting that the nature of the hydride donor does not impact the relative orientation of the bpy and $Acr^+$ rings.

When the full set of $^{R}Acr^+$ acceptors is considered, theoretical calculations exhibit excellent correlation with the experimental measurements for the trends in the thermodynamic hydricities as revealed by the Brønsted plot of ln($K_{eq}$) vs. ln($k_1$), where $K_{eq}$ is the equilibrium constant for the hydride transfer reaction derived from computed relative hydricities of Cp*Ir($^{R}$bpy)$H^+$ complexes and $^{R}Acr^+$ acceptors and $k_1$ is the experimental rate constant for

hydride transfer reaction (Figures S69-S71). These Brønsted plots exhibit essentially the same slopes (Figure S72-S74) as those derived from experimental thermodynamic hydricities (Figure 4) indicating the accurate computational prediction of the relative thermodynamic hydricities. We conclude from this observation that thermodynamic hydricity values reported in the literature[22d] for Cp*Ir($^{R}$bpy)H$^{+}$ and determined in this work for $^{R}$Acr$^{+}$ acceptors are likely accurate.

For kinetic hydricities, the calculations reproduce the observed patterns when a Cp*Ir($^{R}$bpy)H$^{+}$ complex is changed for a given $^{R}$Acr$^{+}$ acceptor, *i.e.* Cp*Ir($^{OMe}$bpy)H$^{+}$ reacts faster than Cp*Ir(bpy)H$^{+}$ and Cp*Ir($^{CO2Me}$bpy)H$^{+}$ (Table S14). However, there is significant scatter in the calculated activation energies when the $^{R}$Acr$^{+}$ acceptors are varied for a given Cp*Ir($^{R}$bpy)H$^{+}$ complex, *i.e.* for Cp*Ir($^{OMe}$bpy)H$^{+}$ the rate of hydride transfer to $^{Me}$Acr$^{+}$ is predicted to be approximately the same as for $^{Br}$Acr$^{+}$. This results in different slopes compared to the experimental Brønsted plots when calculated activation energies are plotted against calculated thermodynamic driving force. To evaluate if these discrepancies arise due to shortcomings with the selected levels of DFT, we carried out further calculations at the DLPNO-CCSD(T) level of theory (see Section SXV). Similar results with scattered activation free energies were observed (Tables S17-S18). Surprisingly, the computed activation free energies in vacuum at all levels of theories provided much improved correlation with the trends observed for experimental rates even partially reproducing the trends in the slopes of Brønsted plots (Figure S81-S84). Although in vacuum the absolute values of activation free energies differ significantly from the experimental measurements (Tables S15-S16), this observation indicates that they provide better prediction for the trends in experimental rates compared to those computed using continuum solvation models. These results also suggest that the discrepancy in the correlation of computed activation free energies and the experimental rates originates from accounting for bulk solvation effects using continuum models rather than the level of theories applied in the present work.

*Application of Marcus Theory to Hydride Transfer from Cp*Ir($^{R}$bpy)H$^{+}$ to Acr$^{+}$*

Given that our experimental and computational results indicate that hydride transfer from Cp*Ir($^{R}$bpy)H$^{+}$ to acridinium acceptors proceeds through a single concerted step, we fitted the data in the Brønsted plot (Figure 4a) for each metal hydride donor (Cp*Ir($^{R}$bpy)H$^{+}$; R = OMe, H, and $CO_2Me$) to the Marcus relation. Specifically, we used Eq 2, which has previously been used to model hydride transfer reactions involving organic donors and acceptors:[17]

$$\ln k_1 = \ln\left(\frac{k_B T}{h}\right) - \left(\frac{W^r}{RT}\right) - \left(\frac{\lambda}{4RT}\right) + \left(\frac{\ln K_{eq}}{2}\right) - \left(\frac{RT(\ln K_{eq})^2}{4\lambda}\right) \qquad (Eq\ 2)$$

where $k_1$ is the rate constant for hydride transfer, $k_B$ is the Boltzmann constant, $T$ is the temperature, $h$ is Planck's constant, $W^r$ is the standard free energy required to bring the reactants together to form a precursor complex (the electrostatic work term), $R$ is the gas constant, $\lambda$ is the reorganization energy, and $K_{eq}$ is the equilibrium constant for the hydride transfer reaction. It has previously been demonstrated that $\lambda$ values are highly sensitive to the value of $W^r$ in hydride transfer reactions involving organic substrates.[16c,31] Given our relatively small data sets, we did not want to treat both $W^r$ and $\lambda$ as variables in Eq 2. Therefore, a previously described method,[32] which required experimental data on the solid-state structures of Cp*Ir(bpy)H$^+$ and Acr$^+$, was used to estimate a $W^r$ value of 0.23 kcal mol$^{-1}$ for a representative hydride transfer reaction between Cp*Ir(bpy)H$^+$ and Acr$^+$ (see Section SXII). The data sets for hydride transfer from Cp*Ir($^{OMe}$bpy)H$^+$, Cp*Ir(bpy)H$^+$, and Cp*Ir($^{CO2Me}$bpy)H$^+$ to Acr$^+$ were then all fitted to Eq 2 using 0.23 kcal mol$^{-1}$ as the $W^r$ value (Figure 7). The fits for Cp*Ir(bpy)H$^+$ and Cp*Ir($^{CO2Me}$bpy)H$^+$ are excellent, while the fit for Cp*Ir($^{OMe}$bpy)H$^+$ is slightly worse. The $\lambda$ values for H$^-$ transfer were estimated to be approximately 58, 65, and 69 kcal mol$^{-1}$ for hydride transfer from Cp*Ir($^{OMe}$bpy)H$^+$, Cp*Ir(bpy)H$^+$, and Cp*Ir($^{CO2Me}$bpy)H$^+$, respectively. When the value of $W^r$ is increased, the value of $\lambda$ decreases, but the trends between compounds remain the same, so Cp*Ir($^{OMe}$bpy)H$^+$ gives lower $\lambda$ values than Cp*Ir(bpy)H$^+$, and Cp*Ir($^{CO2Me}$bpy)H$^+$. Further, the absolute change in $\lambda$ is relatively small as $W^r$ is varied. For example, when a $W^r$ value of 2.5 kcal mol$^{-1}$ is used for Cp*Ir($^{OMe}$bpy)H$^+$, $\lambda$ is predicted to be 48 kcal mol$^{-1}$. In this case, there is a slightly better fit of the data to Eq 2 (Figure S66), suggesting that the estimated value of $W^r$ 0.23 kcal mol$^{-1}$ may be an underestimate. In contrast,

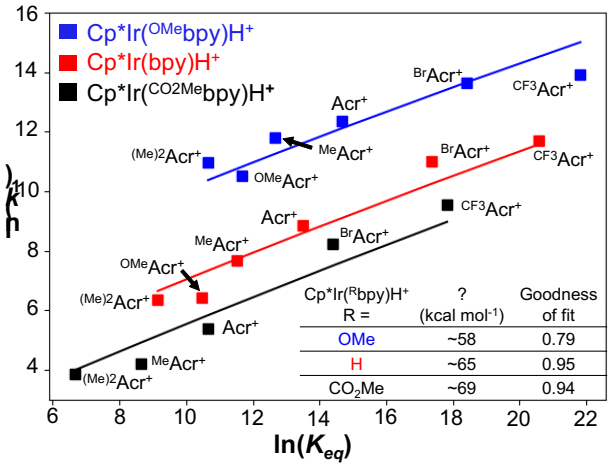


**Figure 7:** Marcus fits for H$^-$ transfer from Cp*Ir($^{R}$bpy)H$^+$ (R = OMe, H, and $CO_2Me$) hydride donors to acridinium acceptors $^{R}$Acr$^+$ (R = $(Me)_2$, OMe, Me, H, Br, and $CF_3$). All the data were fitted to the Marcus relation shown in Eq 2 with $W^r$ = 0.23 kcal mol$^{-1}$.

the fits for Cp*Ir(bpy)$H^+$ and Cp*Ir($^{CO2Me}$bpy)$H^+$ are worse when a value for $W^r$ of 2.5 kcal $mol^{-1}$ is used, suggesting that a lower estimate of $W^r$ is better for these systems. This indicates that even if the values of $W^r$ are different for all three complexes, the trend of Cp*Ir($^{OMe}$bpy)$H^+$ giving a lower $\lambda$ values than Cp*Ir(bpy)$H^+$ and Cp*Ir($^{CO2Me}$bpy)$H^+$ is likely correct. We also estimated $W^r$ computationally for the reactions of $Acr^+$ with Cp*Ir($^{R}$bpy)H but using these values gave worse fits to Eq 2, and consequently this approach was not pursued further (Table S21).

In outer sphere electron transfer reactions $\lambda$ has been estimated computationally using Eq 3:[10,33]

$$\lambda = \lambda_{int} + \lambda_s \quad (Eq\ 3)$$

where $\lambda_{int}$ accounts for the internal molecular structural changes, and $\lambda_s$ accounts for the solvent reorganization energy. To support the values derived from experimental data, we determined $\lambda$ computationally by performing geometry optimizations at the $r^2$-SCAN-3c level of theory[34] in vacuum, followed by single point calculations at the B3LYP-D3BJ level in conjunction with the CPCM solvation model[35] for a reaction between Cp*Ir(bpy)$H^+$ and $Acr^+$ (Eq S8). A modified version of the four-point scheme for electron transfer[36] was used to calculate that $\lambda_{int}$ is 37.2 kcal $mol^{-1}$ and a two-sphere model[10] applied for $\lambda_s$, which yielded estimated values between 9-19 kcal $mol^{-1}$ depending on the assigned value for the separation distance between Cp*Ir(bpy)$H^+$ and $Acr^+$ (5 Å to 7 Å) (Table S20). This leads to a calculated λ value of approximately 58-68 kcal $mol^{-1}$ (with the inclusion of the free energy of solvent coordination to the metal center after hydride transfer, $\Delta G = -10.6$ kcal $mol^{-1}$; Figure S85)[37] suggesting that we have a solid model, given the inherent challenges associated with calculating $\lambda$[38] and the sensitivity of $\lambda$ to $W^r$. We note that as we contract the separation distance between the spheres representing Cp*Ir(bpy)$H^+$ and $Acr^+$ in the the two sphere model, the $\lambda_s$ value approaches zero and the variation in distance is the source of the large uncertainty in the estimation (Table S20). To gain further insight about $\lambda$, we developed models of reactant and product complexes in the presence of sixty explicit solvent molecules (Figure S85) and estimated a $\lambda_s$ value of 3.7 kcal $mol^{-1}$ and a $\lambda_{int}$ value of 48.8 kcal $mol^{-1}$ (excluding explicit solvent molecules and including the free energy of solvent binding after hydride transfer). This yields a calculated $\lambda$ of ~53 kcal $mol^{-1}$ for $\lambda$, which is in reasonable agreement with experiment and our computational model without explicit solvent molecules. The relatively small magnitude of $\lambda_s$ compared to $\lambda_{int}$ is in line with the inner-sphere nature of the hydride transfer reaction.

## Discussion

*Correlation Between Thermodynamic Driving Force and Kinetics of Hydride Transfer*

In this work, we have completed the first correlations between kinetic and thermodynamic hydricity for a metal complex using *only experimental data*. It is challenging to perform this type of study because both kinetic and thermodynamic hydricity are difficult to measure.[8e] For example, to determine kinetic hydricity, it is necessary to find synthetically accessible, tunable, and stable hydride donors and acceptors that undergo clean hydride transfer reactions at rates that can be measured spectroscopically. Further, to correlate kinetic and thermodynamic hydricity successfully across a range of complexes, all measurements must be performed in the same solvent and the electronic properties of the donor and acceptor need to be modified without varying the steric properties.[20e] Using Cp*Ir($^{R}$bpy)H$^{+}$ type hydride donors and $^{R}$Acr$^{+}$ as hydride acceptors, which are both stable in MeCN, we have met these demanding criteria.

An initial analysis of the relationship between kinetic and thermodynamic hydricity for hydride transfer from Cp*Ir($^{R}$bpy)H$^{+}$ to $^{R}$Acr$^{+}$ was conducted using plots of ln($k_1$) vs ln($K_{eq}$). These Brønsted plots can be analyzed without knowledge of the detailed mechanism of hydride transfer, and it is valuable to probe the relationship in this way before introducing mechanism-dependent Marcus analysis. In our case, Brønsted plots clearly show that there are LFERs between thermodynamic driving force and the rate of hydride transfer between Cp*Ir($^{R}$bpy)H$^{+}$ and the acridinium acceptors ($^{R}$Acr$^{+}$) with the rate of hydride transfer increasing as the thermodynamic driving force of the reaction increases (Figure 4). A surprising finding is immediately apparent from Figure 4: our data reveals that each individual Cp*Ir($^{R}$bpy)H$^{+}$ complex follows its own LFER, rather than all combinations of metal hydride and organic acceptors obeying the same relationship. For example, we observe that at the same driving force hydride transfer reactions involving an Ir complex with a more electron rich bpy ligand, Cp*Ir($^{OMe}$bpy)H$^{+}$, occurs significantly faster than those with less electron rich bpy ligands.

Our distinct LFERs stand in contrast to the seminal results from Kreevoy for organic hydride donors and acceptors,[16c] which suggest that rates for a wide range of organic hydride donors and acceptors depend only on the thermodynamic driving force (Figure 1a). Instead, our results are most consistent with Lee *et al.*'s work for hydride transfer for organic systems (Figure 1b),[16i] which show different LFERs depending on the structure of the acceptor and donor, but that a given donor will display an LFER with a group of acceptors. However, further analysis of Kreevoy's data reveal that the fits for a single donor with a set of acceptors are better than for all donors (Figures S67-S68) and it is likely because the data set is so wide that the scatter

for structurally different donors is less apparent. Hence, the trends we observe are also captured in Kreevoy's work and it is likely always the case that structurally similar donors and acceptors give better correlations.

Analysis of the LFERs for the three different Ir hydride donors reveals a less steep Brønsted slope ($\alpha$ = ~0.3) for Cp*Ir($^{OMe}$bpy)H$^+$ compared to either Cp*Ir($^{R}$bpy)H$^+$ (R = H and $CO_2Me$) ($\alpha$ = ~0.5). This indicates that a greater change in thermodynamic hydricity is required to accelerate the rate of hydride transfer from Cp*Ir($^{OMe}$bpy)H$^+$ compared to Cp*Ir($^{R}$bpy)H$^+$ (R = H and $CO_2Me$). The observed $\alpha$ values are within the range observed for hydride transfer between organic hydride donors and acceptors and are broadly consistent with a pathway involving concerted hydride transfer.[16a,16c-e] Nevertheless, it is noteworthy that the $\alpha$ value for Cp*Ir($^{OMe}$bpy)H$^+$ is lower than the other complexes. Recent studies on understanding multi-site proton-coupled electron transfer (PCET) reactions have demonstrated that subtle effects related to concerted but asynchronous transfer of the proton and electron can give rise to low $\alpha$ values.[39] Further, in organic hydride transfer reactions an imbalance in the change in the hybridization states of the hydride donor and hydride acceptor along the reaction coordinate has led to atypical behavior.[40] In our case, it is certainly feasible that there is small imbalance in the transition state, which could cause deviations from an $\alpha$ value of 0.5 and that this would be most pronounced for one of the Ir complexes.

When the Brønsted slopes for different acridinium acceptors (Figure 4b) are compared to their hydride affinities, we observe a linear increase in $\alpha$ as the thermodynamic driving force increases (Figure 8). This implies that as the hydride transfer reaction becomes more thermodynamically favorable, the rate of hydride transfer starts to depend less strongly on the

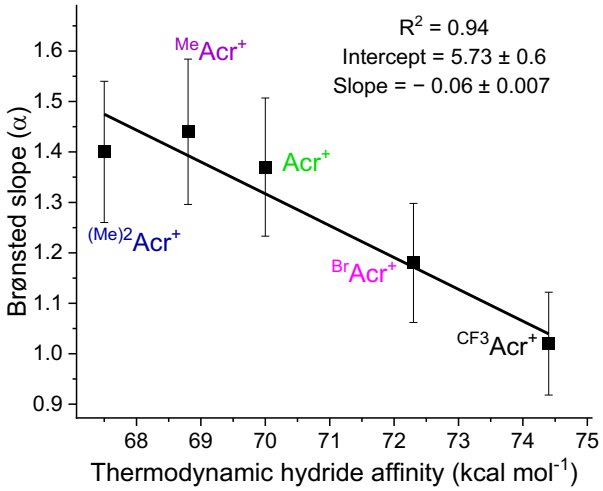


**Figure 8:** Correlation between the slope of Brønsted plots and thermodynamic affinities of acridinium acceptors.

thermodynamic hydricity of the Ir hydride. This observation is consistent with our previous results for hydride donation from ($^{R}$bpy)Re(CO)$_3$H complexes to organic acceptors,[20e] suggesting that the somewhat unexpected linear trend is general. Although the physical reasons for the linear relationship are unclear, the general trend can be explained by considering the nature of the transition state for hydride transfer. In reactions in which there is less thermodynamic driving force the transition state is later and more product like (*vide infra*). Therefore, there is greater cleavage of the Ir–H and more incipient charge on the metal center, which causes there to be a larger influence from the substituents on the bpy ligand. This observation is particularly relevant for catalysis, where it is desirable to run reactions as close to thermoneutral as possible to avoid thermodynamic sinks. A common strategy for achieving this goal is to vary the substituents on the catalyst. For the types of hydride transfer reactions studied in this work it is important to be aware that as a reaction moves further away from thermoneutral changing the substituents on the donor or acceptor will have a smaller influence on the rate.

A feature of our LFERs is that we determined the driving force (ln $K_{eq}$) for the hydride transfer reactions by including both the hydride transfer steps and the binding of MeCN to the Ir complex after hydride transfer (Eq 4). This is because thermodynamic hydricity, which was

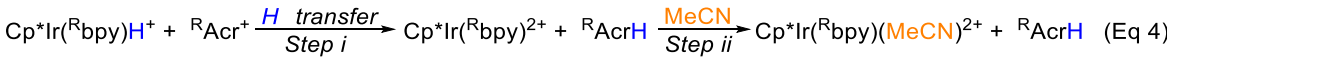

(Eq 4)

used to determine the thermodynamic driving force for the reaction, explicitly considers solvent binding.[8b] It is possible that the differences we observed between the complexes are at least partially related to variation in the strength of MeCN binding to the Ir complexes depending on the substituents on the bpy ligand. Determining the binding constant of MeCN to Cp*Ir($^{R}$bpy)$^{+}$ experimentally is challenging. Therefore, theoretical calculations were performed to estimate the thermodynamic free energy for MeCN binding to the Ir center after the hydride transfer step which resulted in computed ΔG values of -9.9, -9.1 and -6.8 kcal mol$^{-1}$ for Cp*Ir($^{CO2Me}$bpy)$^{2+}$, Cp*Ir(bpy)$^{2+}$, and Cp*Ir($^{OMe}$bpy)$^{2+}$, respectively, using initial geometry optimizations in vacuum at the B3LYP-D3BJ level, followed by MN15 single point calculations with SMD solvation (Table S6). Using this information, revised Brønsted plots were prepared where only the thermodynamic driving force associated with the hydride transfer step was included. These plots result in essentially the same slopes in the Brønsted plots (Figure S65) as observed without the solvent binding correction, indicating that MeCN coordination is

not responsible for the differences between the Ir complexes. Similar results are obtained if calculations are performed using different methods (Figure S65).

In general, we observe that although theory is excellent at reproducing our experimental trends relating to reaction thermodynamics and absolute reaction barriers, it is less effective at reproducing trends related to kinetic factors. Specifically, it cannot capture the subtle variations in the rates of hydride transfer as the $^{R}Acr^{+}$ acceptor is varied for any given Ir complex. However, given that the differences in activation barrier for hydride transfer from various $^{R}Acr^{+}$ acceptors to a given Ir hydride donor are small (between 0.2-2 kcal mol$^{-1}$), it is perhaps unsurprising that this is beyond the accuracy of applied computational methods. One interesting observation is the better reproduction of experimental variations in $\Delta G^{\ddagger}$ related to substituent effects for the acceptor by calculations performed in vacuum, which indicates that the theoretical methods are likely struggling to account for solvation effects. At this stage, we recommend the use of a range of density functionals in conjunction with continuum solvation methods to calculate thermodynamic hydricity, and the MN15 level of theory to predict individual $\Delta G^{\ddagger}$ values for a given hydride transfer reaction. Nevertheless, our inability to accurately reproduce kinetic changes related to substituent effects provides a compelling rationale for the need for experimental kinetic studies to study this type of reaction and the continued development of improved theoretical methods.

*Mechanism of Hydride Transfer Reactions and the Nature of the Transition State*

In principle, hydride transfer from Cp*Ir($^{R}$bpy)H$^{+}$ donors to Acr$^{+}$ acceptors may occur through a single step direct hydride transfer or multi-step reaction pathways involving ET, PT, or HAT as shown in Figure 5. Analysis of the activation parameters for hydride transfer from Cp*Ir($^{R}$bpy)H$^{+}$ to Acr$^{+}$ indicates that the entropy of activation is different for Cp*Ir($^{OMe}$bpy)H$^{+}$ compared to Cp*Ir(bpy)H$^{+}$ or Cp*Ir($^{CO2Me}$bpy)H$^{+}$ (Table 3), which could imply that the reaction

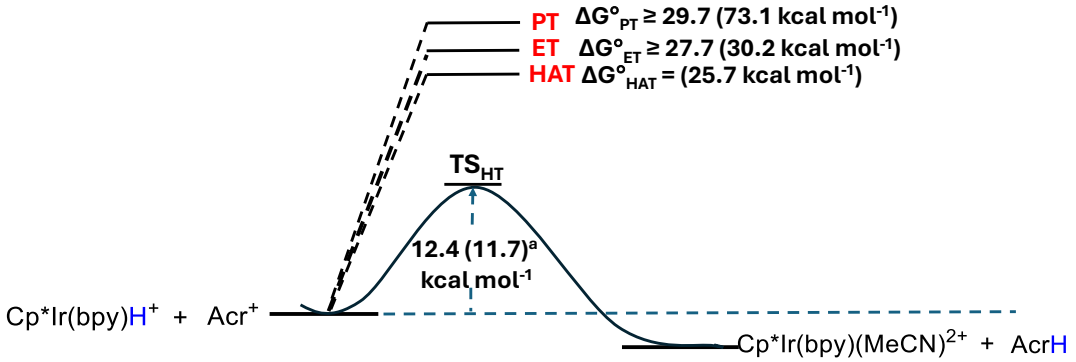


**Figure 9:** Comparison of thermodynamic free energy changes (ΔG°) for pathways involving initial, PT, ET, or HAT for hydride transfer from Cp*Ir(bpy)H$^{+}$ to Acr$^{+}$ and with the experimentally determined barrier for hydride transfer. The values given in parentheses are computationally determined as described in Table 5.

mechanism for hydride transfer from Cp*Ir($^{OMe}$bpy)H$^+$ is different relative to Cp*Ir(bpy)H$^+$ or Cp*Ir($^{CO2Me}$bpy)H$^+$. For example, hydride transfer from Cp*Ir($^{OMe}$bpy)H$^+$ could proceed via a concerted process, while reactions from Cp*Ir(bpy)H$^+$ and Cp*Ir($^{CO2Me}$bpy)H$^+$ could proceed via stepwise processes (or *vice versa*). However, our thermochemical analysis, using experimental and thermochemical methods to determine the possibility of initial PT, ET, or HAT, indicates that the minimum energy required for PT, ET, or HAT, is significantly higher than the reaction barrier (see Figure 9 for Cp*Ir(bpy)H$^+$ and the Tables S2-S5 in the SI for Cp*Ir($^{OMe}$bpy)H$^+$ and Cp*Ir($^{CO2Me}$bpy)H$^+$). On this basis, we propose that all hydride transfer reactions studied in this work are proceeding through a concerted hydride transfer pathway.

The KIEs obtained by comparing the rates of hydride transfer of complexes of the type Cp*Ir($^{R}$bpy)H$^+$ with Cp*Ir($^{R}$bpy)D$^+$ also provide support for a single step concerted hydride transfer. Specifically, comparable KIEs are obtained at a similar thermodynamic driving force for all three Cp*Ir($^{R}$bpy)H$^+$ donors and there is an increase in the KIE for hydride transfer as the reaction becomes more thermodynamically favorable. This is consistent with previous results both from our groups and Bullock and co-workers for reactions that proceed via direct hydride transfer.[20e,27c] The changes from inverse to normal KIE as hydride transfer becomes more thermodynamically favorable for Cp*Ir(bpy)H$^+$ and Cp*Ir($^{CO2Me}$bpy)H$^+$ have also been observed for other systems.[20e,27c] We propose that the slightly higher KIE values observed for the most hydridic Cp*Ir($^{OMe}$bpy)H$^+$ donor, indicate the existence of a more reactant-like transition state structure compared to less hydridic Cp*Ir($^{CO2Me}$bpy)H$^+$ donor. This hypothesis is consistent with the less negative value of activation entropy value obtained in case of Cp*Ir($^{OMe}$bpy)H$^+$, which suggests a stronger interaction of the hydride with the Ir center than the carbon center of acridinium ($C_{Acr+}$) in the transition state structure leading to less order. The KIE values demonstrate that as the thermodynamic driving force for hydride transfer is increased the change in KIE is smaller for Cp*Ir($^{CO2Me}$bpy)H$^+$ compared to Cp*Ir($^{OMe}$bpy)H$^+$. At this stage, we do not have an explanation for this observation and likely high-level calculations that can model the movement of both the proton and the electron are required to fully understand the observed KIEs.[41]

The calculated transition state structures for hydride transfer from Cp*Ir($^{R}$bpy)H$^+$ to $^{R}$Acr$^+$ allows for analysis of the trends in the position of the transition state in relation to the starting material and products (*e.g.* early or late transition states). Figure 10 shows the trends in calculated bond distances of the Ir−H bond and the incipient $C_{Acr}$−H bond in the transition state across all of our Cp*Ir($^{R}$bpy)H$^+$ donors and $^{R}$Acr$^+$ acceptors. This complements the data in

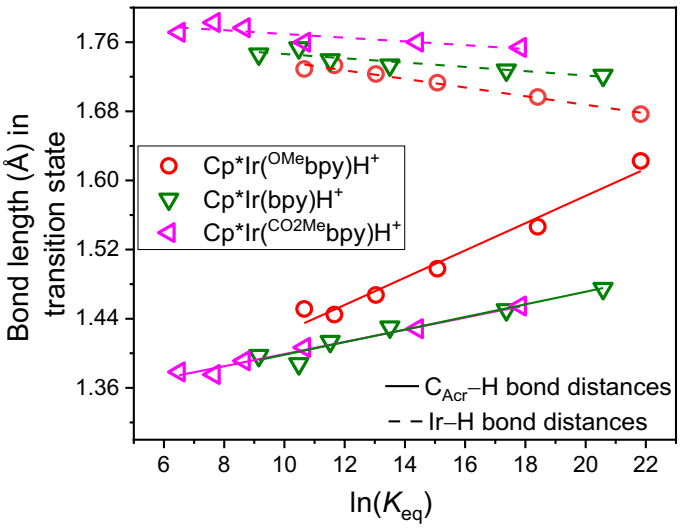


**Figure 10:** Plot showing the trends in the calculated Ir-H and incipient $C_{Acr}$–H bond distances in the transition state for the hydride transfer reactions from Cp*Ir($^{R}$bpy)H$^+$ (R = OMe, H, $CO_2Me$) donors to $^{R}$Acr$^+$ acceptors. The solid and dashed lines show the trend in the $C_{Acr+}$–H and Ir–H bond distances, respectively.

Table 6. As the reaction becomes more thermodynamically favorable the extent of Ir–H bond cleavage decreases and the degree of $C_{Acr}$–H bond formation increases, indicating an earlier transition state. This is consistent with analysis of the transition state for hydride transfer from Cp*Ir($^{R}$bpy)H$^+$ to Acr$^+$ using the IBSI and supports the results from our KIE studies. Our results show that for all three Ir hydride donors, an earlier transition state is observed for $^{R}$Acr$^+$ acceptors with higher hydride affinities, such as $^{CF_3}$Acr$^+$ compared to lower hydride affinities, such as $^{(Me)2}$Acr.

Along with the differences in the Ir–H and $C_{Acr}$–H bond distances between the three Ir donors with any specific $^{R}$Acr$^+$ acceptor, there are also changes in the extent of π-stacking between the bpy plane of Cp*Ir($^{R}$bpy)H$^+$ (R = OMe, H, and $CO_2Me$) and the aromatic rings in $^{R}$Acr$^+$. Although these changes do not follow an obvious pattern, we suggest that these variations contribute to the different lines in the Brønsted plot for Cp*Ir($^{OMe}$bpy)H$^+$, Cp*Ir(bpy)H$^+$, and Cp*Ir($^{CO2Me}$bpy)H$^+$. This is especially the case given that examples involving both multi-site PCET and hydride transfer between organic donors and acceptors establish that subtle effects can exert large and in some cases counterintuitive influences on α even for closely related systems.[39,40]

The hydride transfer reactions studied in this work involve two cationic species and it is possible that aggregation between the cations and anions impact the observed rates. To probe the potential role of ion-pairing, we synthesized the compounds [Cp*Ir(bpy)H][BAr$^F_4$] (BAr$^F_4$ = {3,5-$(CF_3)_2C_6H_3$}$_4$B$^-$) and [Acr][BAr$^F_4$] (see Section SII). The rate of hydride transfer between [Cp*Ir(bpy)H][BAr$^F_4$] and [Acr][BAr$^F_4$] is the same (within error) as for related

compounds with $PF_6$ anions (see Section SXIV). Further, we determined that the KIE for hydride transfer between [Cp*Ir(bpy)H][$BAr^F_4$]/[Cp*Ir(bpy)D][$BAr^F_4$] and [Acr][$BAr^F_4$] is 0.99, the same (within error) as the KIE obtained for compounds with $PF_6$ anions. These results strongly suggest that aggregation is not an issue and the rates we are measuring relate directly to hydride transfer. When the solvent for the reaction was changed from MeCN to a 9:1 (v:v) mixture of α,α,α-trifluorotoluene and MeCN, hydride transfer from Cp*Ir($^{OMe}$bpy)$H^+$ to $Acr^+$ is still significantly faster than from Cp*Ir(bpy)$H^+$ (see Section SXIV). This argues against aggregation effects being significant and suggests that the observed relative differences in rates between the complexes are not related to solvent effects. There is, however, a significant difference in the absolute rate of hydride transfer when the solvent is changed, as previously observed.[26b,42]

*Application of Marcus Theory to Hydride Transfer from Cp*Ir($^R$bpy)$H^+$ donors*

Even though Marcus theory was developed for understanding outer-sphere electron transfer,[10] it has proved effective for modelling many more complicated reactions, such as hydrogen atom transfer[11] and group transfer[12] reactions, and even hydride transfer between organic donors and acceptors.[16] Our ability to fit a Marcus model to the Brønsted plots for hydride transfer from Cp*Ir($^R$bpy)$H^+$ to $Acr^+$ indicates that it can also be applied to a hydride transfer from a metal complex (Figure 7). In fact, to our knowledge this work represents the first occasion when $\lambda$ values have been accurately determined using the elementary rates of hydride transfer for transition metal complexes.[43]

The unique Marcus analysis of transition metal hydride complexes performed here enables several key conclusions to be drawn: (i) The $\lambda$ values for hydride transfer from Cp*Ir($^R$bpy)$H^+$ complexes (< 70 kcal $mol^{-1}$) to organic donors are lower than those typically observed for reactions between organic hydride donors and acceptors >70 kcal $mol^{-1}$). This suggests that, as previously hypothesized in the literature,[17] hydride transfer from a metal complex will be faster than from an organic compound at the same thermodynamic driving force. (ii) The present $\lambda$ values are also consistent with those determined for other hydride transfer reactions involving metal hydrides using the Marcus cross-relation.[21] (iii) Cp*Ir($^{OMe}$bpy)$H^+$ gives faster rates of hydride transfer even at the same thermodynamic driving force as Cp*Ir(bpy)$H^+$ and Cp*Ir($^{CO2Me}$bpy)$H^+$, consistent with its lower $\lambda$ value (58 kcal $mol^{-1}$ versus 65 and 69 kcal $mol^{-1}$, respectively). (iv) There is reasonable agreement between experiment and theory in calculating $W^r$ and $\lambda$ for Cp*Ir(bpy)$H^+$ but further improvement is required in computational models. The need for experimental data to benchmark computational models, which may

eventually enable the use computations to predict of $\lambda$ is a reason for further experimental studies. (v) Finding systems with lower $\lambda$ values will likely be a successful strategy for improving the rates of hydride transfer without changing the thermodynamic driving force, which has applications to $CO_2$ reduction chemistry. For example, it may be desirable to increase the rate of hydride transfer to $CO_2$ but increasing the thermodynamic hydricity of the metal hydride may lead to increased protonation to generate hydrogen. Finding systems with lower $\lambda$ values provides an alternative method to optimize the rate of hydride transfer.[44]

In previous work Wieder *et al*., demonstrated that the Marcus cross-relation held for a hydride transfer reaction between a Rh hydride and organic acceptor.[8b] We wanted to evaluate if the cross-relation also held for our systems. Unfortunately, experimentally, we were unable to accurately measure the rate of exchange between Cp*Ir(bpy)$H^+$ and Cp*Ir($^{CO2Me}$bpy)(MeCN)$^{2+}$, which we aimed to use as an approximate value for the self-exchange rate for hydride transfer between Cp*Ir(bpy)$H^+$ and Cp*Ir(bpy)(MeCN)$^{2+}$. The rate could not be measured because the reaction is very slow, likely because initial MeCN decoordination from Cp*Ir($^{CO2Me}$bpy)(MeCN)$^{2+}$, which is required for hydride transfer is thermodynamically unfavorable. This stands in contrast with our reactions between Cp*Ir($^{R}$bpy)$H^+$ and organic acceptors, where ligand dissociation is not required prior to the

**a)** *Calculated barriers for self-exchange reactions*

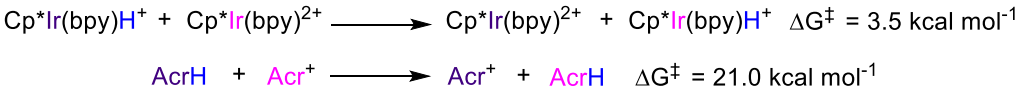


**b)** *Barrier for the cross reaction calculated using the Marcus cross-relation*

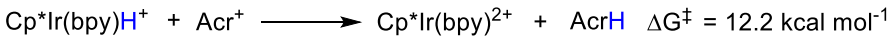


**Figure 11:** Calculated barriers for self-exchange reactions (**a**) that were used in the Marcus cross-relation to predict the barrier for hydride transfer from Cp*Ir(bpy)$H^+$ to $Acr^+$.

hydride transfer step, and rates are fast and possible to measure experimentally. Therefore, using constrained optimizations we estimated the free energy of activation ($\Delta G^{\ddagger}$) for self-exchange between Cp*Ir(bpy)$H^+$ and Cp*Ir(bpy)$^{2+}$ to be 3.5 kcal mol$^{-1}$ (Figure 11) while calculating the barrier for self-exchange for $Acr^+$ with AcrH to be 21.0 kcal mol$^{-1}$ by locating the transition state structures with full optimizations. Using the Marcus cross-relation this suggests that the barrier for hydride transfer from Cp*Ir(bpy)$H^+$ to $Acr^+$ should be 12.2 kcal mol$^{-1}$. This is in excellent agreement with our experimental value ($\Delta G^{\ddagger}_{303} = 12.4 \pm 1.2$ kcal mol$^{-1}$) and indicates that the cross-relation holds, again suggesting that Marcus theory can be used to predict the rates of hydride transfer reactions.

In our Marcus analysis we did not modify the values of $\Delta G^{o}$ (and consequently $K_{eq}$) for hydride

transfer reactions to explicitly include distance dependent Coulombic effects. This is despite previous studies on electron transfer[45] and hydride transfer involving organic species[16c,17] demonstrating that when using Marcus theory to model reactions involving charged reactants and products it may be necessary to include a distance dependent Coulombic correction to ΔGº as defined in Eq 5.

$$\Delta G^{o\prime} = \Delta G^{o} - W^{r} + W^{p} \qquad (Eq\ 5)$$

where $W^r$ and $W^p$ are the standard free energies for the formation of precursor and successor complexes and are distance dependent. In our case $W^p$ is 0 because the organic product is not charged, and we estimate a small value of $W^r$ (*vide supra*). When we use ΔGº' to determine $K_{eq}$ in Eq 2, we see no significant changes in λ and hence for simplicity we have excluded the correction (see Section SXVI). However, if a similar analysis is being performed on a related system involving charged reactants and products it may be necessary to use a Marcus model that explicitly considers distance dependent Coulombic effects on the thermodynamics of the reaction.

Given that Marcus theory was developed to model the rates of outer-sphere electron transfer, and can struggle to model inner-sphere electron transfer,[46] it is surprising that it appears to be effective for inner-sphere hydride transfer. Likely, the inner-sphere nature of the hydride transfer reaction will always limit the generality of the Marcus model for predicting rates. For example, in this work we demonstrate that weak effects such as π-stacking interactions are present in the transition state, which is likely problematic for a purely outer-sphere theory and may contribute to the differences in α and $\lambda$ for the closely related systems studied in this work. Nevertheless, we show that within a range of related compounds that the Marcus model, including the cross-relation, works well and could in principle be used to predict the rates of hydride transfer for a new series of complexes. This is powerful for catalyst design as it indicates that with information about thermodynamics, kinetic effects can be predicted.

**Conclusions**

By using carefully selected hydride donors of type Cp*Ir($^{R}$bpy)H$^+$ and acceptors of the form $^{R}$Acr$^+$ we have explored the kinetics and thermodynamics of hydride transfer between electronically different systems, which have similar steric profiles. The key findings of our study are:

(i) There are clear LFERs between kinetic and thermodynamic hydricity but each Cp*Ir($^{R}$bpy)H$^+$ hydride donor gives a distinct α value in a Brønsted plot. This

demonstrates that in our systems the structure of the donor differentially impacts the rate of hydride transfer. For catalytic applications, it suggests that relatively small electronic variations of the donor could lead to faster rates of hydride transfer at the same thermodynamic driving force.

(ii) As hydride transfer reactions become more thermodynamically favorable, electronic changes to the donor and acceptor have less impact. Hence, modifying the electronic structure of a donor will likely lead to the largest changes in the rate of hydride transfer for thermoneutral reactions.

(iii) Experimental and theoretical analysis suggests that hydride transfer between Cp*Ir($^{R}$bpy)H$^{+}$ and $^{R}$Acr$^{+}$ proceeds via a direct concerted pathway. The transition state for the reaction is earlier for reactions that are more thermodynamically favorable and there is π-stacking between the donor and acceptor in the transition state. Likely, subtle effects such as π-stacking and asynchronicity in the transition state lead to the observed differences in α as the hydride donor is changed.

(iv) Theory is excellent at predicting both absolute and relative thermodynamics but is significantly better at predicting absolute compared to relative kinetics. Likely problems modelling solvation cause theory to be unable to predict relative trends in kinetics between systems with small differences in their electronic properties and improved theoretical methods are required to for the prediction of improved catalysts for reactions where hydride transfer is turnover limiting.

(v) Marcus theory can be used to analyze hydride transfer reactions between Cp*Ir($^{R}$bpy)H$^{+}$ and $^{R}$Acr$^{+}$ and the $\lambda$ values for hydride transfer are significantly smaller for the metal hydride complexes studied in this work compared to organic hydride donors. This indicates that metal hydride donors will inherently be capable of faster rates of hydride transfer in catalysis compared to organic hydride donors and faster systems could be developed by optimizing $\lambda$. In principle, this could be achieved by looking at the rates of self-exchange between a hydride donor and its conjugate acceptor because our results indicate that the Marcus cross-relation holds.

The understanding of hydride transfer from Cp*Ir($^{R}$bpy)H$^{+}$ to $^{R}$Acr$^{+}$ acceptors developed in this work also provides insight into hydride transfer reactions using other metal hydrides and different acceptors. Firstly, we hypothesize that LFERs between kinetic and thermodynamic hydricity will only be present for reactions that proceed via direct concerted hydride transfer and reactions that proceed in a stepwise manner involving either initial PT, ET, or HAT, will

almost certainly follow LFERs involving different thermodynamic properties. In particular, first-row transition metal complexes are more likely to undergo redox processes, and it is important to understand the mechanism of hydride transfer before applying the models derived here to new systems. Secondly, our work suggests that subtle effects such as π-stacking impact the slope of the LFER between kinetic and thermodynamic hydricity and the reorganization energy in Marcus analysis. If a hydride acceptor cannot π-stack, the nature of the LFER even from the same Ir complexes studied in this work are expected to be different. In principle, if secondary sphere effects, such as π-stacking and hydrogen bonding, are not present in the transition state and steric factors are controlled to be uniform, it may be possible to find metal donors and acceptors with different structures that follow a single LFER between thermodynamic and kinetic hydricity. In this case, the reaction thermodynamics will control the kinetics across a range of donor and acceptor structures as observed for electron transfer. Careful computational modelling of transition states will be valuable to find appropriate systems, which will be a goal of future work for our laboratories. Further, for 'real-world' systems with catalytic applications, it is likely that some secondary interactions will be present, which will cause LFERs between kinetic and thermodynamic hydricity to only be valid for closely related donors and acceptors, as observed in this work. This is not surprising given that direct hydride transfer is an inner-sphere process, so the exact structure of the donor and acceptor are expected to influence the reaction barrier. For catalyst design, it is perhaps most important to understand what secondary interactions may be present and then design system that optimize these effects. The creation of LFERs can help with this process.

Overall, this work offers valuable insights into fundamental aspects of hydride transfer reactions involving transition metal hydrides and bridges a critical gap in our understanding of the relationship between kinetic and thermodynamic factors in these reactions. The results provide different strategies for controlling the rates of hydride transfer in both stoichiometric and catalytic reactions and future work will focus on applying our results to catalysis.

**Acknowledgments**

NH acknowledges support from the National Science Foundation through Grant CHE-2347883 and the Yale Center for Natural Carbon Capture. The work at Brookhaven National Laboratory (MZE) was carried out under contract DE-SC0012704 with the U.S. Department of Energy, Office of Science, Office of Basic Energy Sciences, and utilized computational resources at the Center for Functional Nanomaterials, which is a U.S. Department of Energy Office of Science Facility, and the Scientific Data and Computing Center, a component of the Computational

Science Initiative, at Brookhaven National Laboratory under Contract No. DE-SC0012704. Certain aspects of the synthesis and project design relating to Ir hydride complexes were supported by the U.S. Department of Energy, Office of Science, Office of Basic Energy Sciences, under Grant DE-SC0014255 (AJMM). We are grateful to Professor James Mayer for access to his stop-flow instrument and to Dr. Benjamin Groff and Professor James Mayer for valuable discussions. We also acknowledge Dr. Kai Cui for assistance with fitting our data to the Marcus model.

## Supporting Information

Additional experimental details, kinetic data, computational information, characterization details, NMR spectra.

## Competing Financial Interests

The authors declare no competing financial interests.

## References

1. (a) Hoskin, A. J.; Stephan, D. W. Early Transition Metal Hydride Complexes: Synthesis and Reactivity. *Coord. Chem. Rev.* **2002**, *233*, 107; (b) McGrady, G. S.; Guilera, G. The Multifarious World of Transition Metal Hydrides. *Chem. Soc. Rev.* **2003**, *32*, 383; (c) Samec, J. S.; Bäckvall, J.-E.; Andersson, P. G.; Brandt, P. Mechanistic Aspects of Transition Metal-Catalyzed Hydrogen Transfer Reactions. *Chem. Soc. Rev.* **2006**, *35*, 237; (d) Norton, J. R.; Sowa, J. Introduction: Metal Hydrides. *Chem. Rev.* **2016**, *116*, 8315; (e) Humphries, T. D.; Sheppard, D. A.; Buckley, C. E. Recent Advances in the 18-Electron Complex Transition Metal Hydrides of Ni, Fe, Co and Ru. *Coord. Chem. Rev.* **2017**, *342*, 19; (f) Ai, W.; Zhong, R.; Liu, X.; Liu, Q. Hydride Transfer Reactions Catalyzed by Cobalt Complexes. *Chem. Rev.* **2018**, *119*, 2876.
2. (a) Bäckvall, J.-E. Transition Metal Hydrides as Active Intermediates in Hydrogen Transfer Reactions. *J. Organomet. Chem.* **2002**, *652*, 105; (b) Blaser, H. U.; Malan, C.; Pugin, B.; Spindler, F.; Steiner, H.; Studer, M. Selective Hydrogenation for Fine Chemicals: Recent Trends and New Developments. *Adv. Synth. Catal.* **2003**, *345*, 103; (c) Johnson, N. B.; Lennon, I. C.; Moran, P. H.; Ramsden, J. A. Industrial-Scale Synthesis and Applications of Asymmetric Hydrogenation Catalysts. *Acc. Chem. Res.* **2007**, *40*, 1291; (d) Wang, D.; Astruc, D. The Golden Age of Transfer Hydrogenation. *Chem. Rev.* **2015**, *115*, 6621; (e) Seo, C. S.; Morris, R. H. Catalytic Homogeneous Asymmetric Hydrogenation: Successes and Opportunities. *Organometallics* **2018**, *38*, 47; (f) Baidilov, D.; Hayrapetyan, D.; Khalimon, A. Y. Recent Advances in Homogeneous Base-Metal-Catalyzed Transfer Hydrogenation Reactions. *Tetrahedron* **2021**, *98*, 132435.
3. (a) Hilt, G. Double Bond Isomerisation and Migration—New Playgrounds for Transition Metal-Catalysis. *ChemCatChem* **2014**, *6*, 2484; (b) Larionov, E.; Li, H.; Mazet, C. Well-Defined Transition Metal Hydrides in Catalytic Isomerizations. *Chem. Commun.* **2014**, *50*, 9816; (c) Hassam, M.; Taher, A.; Arnott, G. E.; Green, I. R.; van Otterlo, W. A. L. Isomerization of Allylbenzenes. *Chem. Rev.* **2015**, *115*, 5462; (d) Vasseur, A.; Bruffaerts, J.; Marek, I. Remote Functionalization Through Alkene Isomerization. *Nature Chem.* **2016**, *8*, 209; (e) Massad, I.; Marek, I. Alkene Isomerization through Allylmetals as a Strategic Tool in Stereoselective Synthesis. *ACS Catal.* **2020**, *10*, 5793; (f) Fiorito, D.; Scaringi, S.; Mazet, C. Transition Metal-Catalyzed Alkene Isomerization as an Enabling Technology in Tandem, Sequential and Domino Processes. *Chem. Soc. Rev.* **2021**, *50*, 1391.
4. (a) Franke, R.; Selent, D.; Börner, A. Applied Hydroformylation. *Chem. Rev.* **2012**, *112*, 5675; (b) Wu, X.-F.; Fang, X.; Wu, L.; Jackstell, R.; Neumann, H.; Beller, M. Transition-Metal-Catalyzed Carbonylation Reactions of Olefins and Alkynes: A Personal Account. *Acc. Chem. Res.* **2014**, *47*, 1041; (c) Clarke, M. L. Hydroformylation. Fundamentals, Processes, and Applications in Organic Synthesis. By Armin Börner and Robert Franke. *Angew. Chem. Int. Ed.* **2016**, *55*, 13377; (d) Nurttila, S. S.; Linnebank, P. R.; Krachko, T.; Reek, J. N. H. Supramolecular Approaches To Control Activity and Selectivity in Hydroformylation Catalysis. *ACS Catal.* **2018**, *8*, 3469; (e) Chakrabortty, S.; Almasalma, A. A.; de Vries, J. G. Recent Developments in Asymmetric Hydroformylation. *Catal. Sci. Technol.* **2021**, *11*, 5388; (f) Rodrigues, F. M. S.; Carrilho, R. M. B.; Pereira, M. M. Reusable Catalysts for Hydroformylation-Based Reactions. *Eur. J. Inorg. Chem.* **2021**, *2021*, 2294.

5. (a) Nakajima, Y.; Shimada, S. Hydrosilylation Reaction of Olefins: Recent Advances and Perspectives. *RSC Adv.* **2015**, *5*, 20603; (b) Du, X.; Huang, Z. Advances in Base-Metal-Catalyzed Alkene Hydrosilylation. *ACS Catal.* **2017**, *7*, 1227; (c) Obligacion, J. V.; Chirik, P. J. Earth-Abundant Transition Metal Catalysts for Alkene Hydrosilylation and Hydroboration. *Nature Rev. Chem.* **2018**, *2*, 15; (d) de Almeida, L. D.; Wang, H.; Junge, K.; Cui, X.; Beller, M. Recent Advances in Catalytic Hydrosilylations: Developments Beyond Traditional Platinum Catalysts. *Angew. Chem. Int. Ed.* **2021**, *60*, 550.
6. (a) Cokoja, M.; Bruckmeier, C.; Rieger, B.; Herrmann, W. A.; Kühn, F. E. Transformation of Carbon Dioxide with Homogeneous Transition-Metal Catalysts: A Molecular Solution to a Global Challenge? *Angew. Chem. Int. Ed.* **2011**, *50*, 8510; (b) Goeppert, A.; Czaun, M.; Jones, J.-P.; Surya Prakash, G. K.; Olah, G. A. Recycling of Carbon Dioxide to Methanol and Derived Products – Closing the Loop. *Chem. Soc. Rev.* **2014**, *43*, 7995; (c) Li, Y.-N.; Ma, R.; He, L.-N.; Diao, Z.-F. Homogeneous Hydrogenation of Carbon Dioxide to Methanol. *Catal. Sci. Technol.* **2014**, *4*, 1498; (d) Wang, W.-H.; Himeda, Y.; Muckerman, J. T.; Manbeck, G. F.; Fujita, E. $CO_2$ Hydrogenation to Formate and Methanol as an Alternative to Photo- and Electrochemical $CO_2$ Reduction. *Chem. Rev.* **2015**, *115*, 12936; (e) Klankermayer, J.; Wesselbaum, S.; Beydoun, K.; Leitner, W. Selective Catalytic Synthesis Using the Combination of Carbon Dioxide and Hydrogen: Catalytic Chess at the Interface of Energy and Chemistry. *Angew. Chem. Int. Ed.* **2016**, *55*, 7296; (f) Bernskoetter, W. H.; Hazari, N. Reversible Hydrogenation of Carbon Dioxide to Formic Acid and Methanol: Lewis Acid Enhancement of Base Metal Catalysts. *Acc. Chem. Res.* **2017**, *50*, 1049; (g) Sordakis, K.; Tang, C.; Vogt, L. K.; Junge, H.; Dyson, P. J.; Beller, M.; Laurenczy, G. Homogeneous Catalysis for Sustainable Hydrogen Storage in Formic Acid and Alcohols. *Chem. Rev.* **2018**, *118*, 372.
7. Dobereiner, G. E.; Crabtree, R. H. Dehydrogenation as a Substrate-Activating Strategy in Homogeneous Transition-Metal Catalysis. *Chem. Rev.* **2010**, *110*, 681.
8. (a) McSkimming, A.; Colbran, S. B. The Coordination Chemistry of Organo-Hydride Donors: New Prospects for Efficient Multi-Electron Reduction. *Chem. Soc. Rev.* **2013**, *42*, 5439; (b) Wiedner, E. S.; Chambers, M. B.; Pitman, C. L.; Bullock, R. M.; Miller, A. J. M.; Appel, A. M. Thermodynamic Hydricity of Transition Metal Hydrides. *Chem. Rev.* **2016**, *116*, 8655; (c) Ilic, S.; Alherz, A.; Musgrave, C. B.; Glusac, K. D. Thermodynamic and Kinetic Hydricities of Metal-Free Hydrides. *Chem. Soc. Rev.* **2018**, *47*, 2809; (d) Waldie, K. M.; Ostericher, A. L.; Reineke, M. H.; Sasayama, A. F.; Kubiak, C. P. Hydricity of Transition-Metal Hydrides: Thermodynamic Considerations for $CO_2$ Reduction. *ACS Catal.* **2018**, *8*, 1313; (e) Brereton, K. R.; Smith, N. E.; Hazari, N.; Miller, A. J. M. Thermodynamic and Kinetic Hydricity of Transition Metal Hydrides. *Chem. Soc. Rev.* **2020**, *49*, 7929.
9. (a) Mochida, I.; Yoneda, Y. Linear Free Energy Relationships In Heterogeneous Catalysis: I. Dealkylation of Alkylbenzenes on Cracking Catalysts. *J. Catal.* **1967**, *7*, 386; (b) Bjelic, S.; Åqvist, J. Catalysis and Linear Free Energy Relationships in Aspartic Proteases. *Biochemistry* **2006**, *45*, 7709; (c) Miller, J. J.; Sigman, M. S. Quantitatively Correlating the Effect of Ligand-Substituent Size in Asymmetric Catalysis Using Linear Free Energy Relationships. *Angew. Chem. Int. Ed.* **2008**, *47*, 771; (d) Pothupitiya, J. U.; Hewawasam, R. S.; Kiesewetter, M. K. Urea and Thiourea H-bond Donating Catalysts for Ring-Opening Polymerization: Mechanistic Insights via (Non) Linear Free Energy Relationships. *Macromolecules* **2018**, *51*, 3203; (e) Lan, Z.; Sharada, S. M. A Framework for Constructing Linear Free Energy Relationships to Design Molecular Transition Metal Catalysts. *Phys. Chem. Chem. Phys.* **2021**, *23*, 15543.
10. Marcus, R. A. Chemical and Electrochemical Electron-Transfer Theory. *Annu. Rev. Phys. Chem.* **1964**, *15*, 155.
11. (a) Roth, J. P.; Yoder, J. C.; Won, T.-J.; Mayer, J. M. Application of the Marcus Cross Relation to Hydrogen Atom Transfer Reactions. *Science* **2001**, *294*, 2524; (b) Warren, J. J.; Mayer, J. M. Predicting Organic Hydrogen Atom Transfer Rate Constants Using the Marcus Cross Relation. *Proc. Natl. Acad. Sci.* **2010**, *107*, 5282; (c) Mayer, J. M. Understanding Hydrogen Atom Transfer: From Bond Strengths to Marcus Theory. *Acc. Chem. Res.* **2011**, *44*, 36; (d) Mayer, J. M. Simple Marcus-Theory-Type Model for Hydrogen-Atom Transfer/Proton-Coupled Electron Transfer. *J. Phys. Chem. Lett.* **2011**, *2*, 1481.
12. (a) Leussing, D. L.; Emly, M. Application of Marcus Theory to Metal Ion Catalyzed Group Transfer Reactions. *J. Am. Chem. Soc.* **1984**, *106*, 443; (b) Lewis, E. S. Application of the Marcus Equation to Methyl Transfers. *J. Phys. Chem.* **1986**, *90*, 3756.
13. (a) Wolfe, S.; Mitchell, D. J.; Schlegel, H. B. Theoretical Studies of $S_N2$ Transition States. 2. Intrinsic Barriers, Rate-Equilibrium Relationships, and the Marcus Equation. *J. Am. Chem. Soc.* **1981**, *103*, 7694; (b) Schlesener, C. J.; Amatore, C.; Kochi, J. K. Kinetics and Mechanism of Aromatic Oxidative Substitutions via Electron Transfer. Application of Marcus Theory to Organic Processes in the Endergonic Region. *J. Am. Chem. Soc.* **1984**, *106*, 3567; (c) Schlesener, C. J.; Amatore, C.; Kochi, J. K. Marcus theory in organic chemistry. Mechanisms of electron and proton transfers from aromatics and their cation radicals. *J. Phys. Chem.* **1986**, *90*, 3747; (d) Zwickl, J.; Shenvi, N.; Schmidt, J. R.; Tully, J. C. Transition State Barriers in Multidimensional Marcus Theory. *J. Phys. Chem. A* **2008**, *112*, 10570.
14. (a) Wu, A.; Mayer, J. M. Hydrogen Atom Transfer Reactions of a Ruthenium Imidazole Complex: Hydrogen Tunneling and the Applicability of the Marcus Cross Relation. *J. Am. Chem. Soc.* **2008**, *130*, 14745; (b) Bím, D.;

Maldonado-Domínguez, M.; Rulíšek, L.; Srnec, M. Beyond the Classical Thermodynamic Contributions to Hydrogen Atom Abstraction Reactivity. *Proc. Natl. Acad. Sci.* **2018**, *115*, E10287; (c) Coste, S. C.; Brezny, A. C.; Koronkiewicz, B.; Mayer, J. M. C–H Oxidation in Fluorenyl Benzoates Does not Proceed Through a Stepwise Pathway: Revisiting Asynchronous Proton-Coupled Electron Transfer. *Chem. Sci.* **2021**, *12*, 13127.
15. (a) Marcus, R. A. Theory of Electron-Transfer Reaction Rates of Solvated Electrons. *J. Chem. Phys.* **1965**, *43*, 3477; (b) Matyushov, D. V. Solvent Reorganization Energy of Electron-Transfer Reactions in Polar Solvents. *J. Chem. Phys.* **2004**, *120*, 7532.
16. (a) Kreevoy, M. M.; Lee, I. S. H. Marcus Theory of a Perpendicular Effect on Alpha for Hydride Transfer Between $NAD^+$ Analogs. *J. Am. Chem. Soc.* **1984**, *106*, 2550; (b) Kreevoy, M. M.; Ostovic, D.; Truhlar, D. G.; Garrett, B. C. Phenomenological Manifestations of Large-Curvature Tunneling in Hydride-Transfer Reactions. *J. Phys. Chem.* **1986**, *90*, 3766; (c) Kreevoy, M. M.; Ostovic, D.; Lee, I. S. H.; Binder, D. A.; King, G. W. Structure Sensitivity of the Marcus Lambda for Hydride Transfer Between $NAD^+$ Analogs. *J. Am. Chem. Soc.* **1988**, *110*, 524; (d) Kim, D.; Lee, I. S. H.; Kreevoy, M. M. The Marcus Theory of the Reactions of Quinolinium Ions with Borohydride and Hydroxide. *J. Am. Chem. Soc.* **1990**, *112*, 1889; (e) Kim, Y.; Truhlar, D. G.; Kreevoy, M. M. An Experimentally Based Family of Potential Energy Surfaces for Hydride Transfer Between $NAD^+$ Analogs. *J. Am. Chem. Soc.* **1991**, *113*, 7837; (f) Lee, I.-S. H.; Jeoung, E. H.; Kreevoy, M. M. Marcus Theory of a Parallel Effect on α for Hydride Transfer Reaction between $NAD^+$ Analogues. *J. Am. Chem. Soc.* **1997**, *119*, 2722; (g) Lee, I.-S. H.; Jeoung, E. H. Reactivities of Five-Membered Heterocycles in Hydride Transfer Reactions. *J. Org. Chem.* **1998**, *63*, 7275; (h) Würthwein, E.-U.; Lang, G.; Schappele, L. H.; Mayr, H. Rate-Equilibrium Relationships in Hydride Transfer Reactions: The Role of Intrinsic Barriers. *J. Am. Chem. Soc.* **2002**, *124*, 4084; (i) Lee, I.-S. H.; Kil, H. J.; Ji, Y. R. Reactivities of Acridine Compounds in Hydride Transfer Reactions. *J. Phys. Org. Chem.* **2007**, *20*, 484.
17. Weerasooriya, R. B.; Gesiorski, J. L.; Alherz, A.; Ilic, S.; Hargenrader, G. N.; Musgrave, C. B.; Glusac, K. D. Kinetics of Hydride Transfer from Catalytic Metal-Free Hydride Donors to $CO_2$. *J. Phys. Chem. Lett.* **2021**, *12*, 2306.
18. Ilic, S.; Gesiorski, J. L.; Weerasooriya, R. B.; Glusac, K. D. Biomimetic Metal-Free Hydride Donor Catalysts for $CO_2$ Reduction. *Acc. Chem. Res.* **2022**, *55*, 844.
19. Gębicki, J.; Marcinek, A.; Zielonka, J. Transient Species in the Stepwise Interconversion of NADH and $NAD^+$. *Acc. Chem. Res.* **2004**, *37*, 379.
20. (a) Matsubara, Y.; Fujita, E.; Doherty, M. D.; Muckerman, J. T.; Creutz, C. Thermodynamic and Kinetic Hydricity of Ruthenium(II) Hydride Complexes. *J. Am. Chem. Soc.* **2012**, *134*, 15743; (b) Sarker, N.; Bruno, J. W. Thermodynamic and Kinetic Studies of Hydride Transfer for a Series of Molybdenum and Tungsten Hydrides. *J. Am. Chem. Soc.* **1999**, *121*, 2174; (c) Ellis, W. W.; Raebiger, J. W.; Curtis, C. J.; Bruno, J. W.; DuBois, D. L. Hydricities of BzNADH, $C_5H_5Mo(PMe_3)(CO)_2H$, and $C_5Me_5Mo(PMe_3)(CO)_2H$ in Acetonitrile. *J. Am. Chem. Soc.* **2004**, *126*, 2738; (d) Nijamudheen, A.; Kanega, R.; Onishi, N.; Himeda, Y.; Fujita, E.; Ertem, M. Z. Distinct Mechanisms and Hydricities of Cp*Ir-Based $CO_2$ Hydrogenation Catalysts in Basic Water. *ACS Catal.* **2021**, *11*, 5776; (e) Espinosa, M. R.; Ertem, M. Z.; Barakat, M.; Bruch, Q. J.; Deziel, A. P.; Elsby, M. R.; Hasanayn, F.; Hazari, N.; Miller, A. J. M.; Pecoraro, M. V.; Smith, A. M.; Smith, N. E. Correlating Thermodynamic and Kinetic Hydricities of Rhenium Hydrides. *J. Am. Chem. Soc.* **2022**, *144*, 17939.
21. Chirila, A.; Hu, Y.; Linehan, J. C.; Dixon, D. A.; Wiedner, E. S. Thermodynamic and Kinetic Activity Descriptors for the Catalytic Hydrogenation of Ketones. *J. Am. Chem. Soc.* **2024**, *146*, 6866.
22. (a) Miller, A. J. M.; Heinekey, D. M.; Mayer, J. M.; Goldberg, K. I. Catalytic Disproportionation of Formic Acid to Generate Methanol. *Angew. Chem. Int. Ed.* **2013**, *52*, 3981; (b) Barrett, S. M.; Pitman, C. L.; Walden, A. G.; Miller, A. J. M. Photoswitchable Hydride Transfer from Iridium to 1-Methylnicotinamide Rationalized by Thermochemical Cycles. *J. Am. Chem. Soc.* **2014**, *136*, 14718; (c) Sasayama, A. F.; Moore, C. E.; Kubiak, C. P. Electronic Effects on the Catalytic Disproportionation of Formic Acid to Methanol by $[Cp^*Ir^{III}(R\text{-bpy})Cl]Cl$ Complexes. *Dalton Trans.* **2016**, *45*, 2436; (d) Brereton, K. R.; Jadrich, C. N.; Stratakes, B. M.; Miller, A. J. M. Thermodynamic Hydricity across Solvents: Subtle Electronic Effects and Striking Ligation Effects in Iridium Hydrides. *Organometallics* **2019**, *38*, 3104; (e) Barrett, S. M.; Stratakes, B. M.; Chambers, M. B.; Kurtz, D. A.; Pitman, C. L.; Dempsey, J. L.; Miller, A. J. M. Mechanistic Basis for Tuning Iridium Hydride Photochemistry from $H_2$ Evolution to Hydride Transfer Hydrodechlorination. *Chem. Sci.* **2020**, *11*, 6442.
23. Pitman, C. L.; Brereton, K. R.; Miller, A. J. M. Aqueous Hydricity of Late Metal Catalysts as a Continuum Tuned by Ligands and the Medium. *J. Am. Chem. Soc.* **2016**, *138*, 2252.
24. Strauss, S. H. The Search for Larger and More Weakly Coordinating Anions. *Chem. Rev.* **1993**, *93*, 927.
25. (a) Pang, X.; Lou, Z.; Li, M.; Wen, L.; Chen, C. Tandem Arylation/Friedel–Crafts Reactions of o-Acylanilines with Diaryliodonium Salts: A Modular Synthesis of Acridine Derivatives. *Eur. J. Org. Chem.* **2015**, *2015*, 3361; (b) Shen, G.-B.; Xia, K.; Li, X.-T.; Li, J.-L.; Fu, Y.-H.; Yuan, L.; Zhu, X.-Q. Prediction of Kinetic Isotope Effects for Various Hydride Transfer Reactions Using a New Kinetic Model. *J. Phys. Chem. A* **2016**, *120*, 1779; (c) Li, Y.; Xu, L.; Wei, Y. Synthesis of Acridines via Copper-Catalyzed Amination/Annulation Cascades Between Arylboronic Acids and Anthranils. *Org. Biomol. Chem.* **2022**, *20*, 9742.

26. (a) Cheng, T.-Y.; Brunschwig, B. S.; Bullock, R. M. Hydride Transfer Reactions of Transition Metal Hydrides: Kinetic Hydricity of Metal Carbonyl Hydrides. *J. Am. Chem. Soc.* **1998**, *120*, 13121; (b) Elsby, M. R.; Espinosa, M. R.; Ertem, M. Z.; Deziel, A. P.; Hazari, N.; Miller, A. J. M.; Paulus, A. H.; Pecoraro, M. V. Carbon Dioxide Insertion into Rhenium Hydrides as a Probe for the Impact of Solvent on Linear Free Energy Relationships between Thermodynamic and Kinetic Hydricity. *Organometallics* **2023**, *42*, 3005.
27. (a) Ostovic, D.; Roberts, R. M. G.; Kreevoy, M. M. Isotope Effects on Hydride Transfer Between $NAD^+$ Analogs. *J. Am. Chem. Soc.* **1983**, *105*, 7629; (b) Kil, H. J.; Lee, I.-S. H. Primary Kinetic Isotope Effects on Hydride Transfer from Heterocyclic Compounds to $NAD^+$ Analogues. *J. Phys. Chem. A* **2009**, *113*, 10704; (c) Cheng, T.-Y.; Bullock, R. M. Isotope Effects on Hydride Transfer Reactions from Transition Metal Hydrides to Trityl Cation. An Inverse Isotope Effect for a Hydride Transfer. *J. Am. Chem. Soc.* **1999**, *121*, 3150.
28. The thermodynamic driving forces for ET are approximations because the oxidation and reduction events of $Cp^*Ir(^Rbpy)H^+$ donors and $^RAcr^+$ acceptors are irreversible. This indicates that the systems are not at thermodynamic equilibrium. Nevertheless, given the close agreement between the experimental values of $\Delta G°_{ET}$ derived from the redox potentials and the computational values of $\Delta G°_{ET}$, this approximation likely does not result in a large error.
29. Klein, J.; Khartabil, H.; Boisson, J.-C.; Contreras-García, J.; Piquemal, J.-P.; Hénon, E. New Way for Probing Bond Strength. *J. Phys. Chem. A* **2020**, *124*, 1850.
30. Deng, J.-H.; Luo, J.; Mao, Y.-L.; Lai, S.; Gong, Y.-N.; Zhong, D.-C.; Lu, T.-B. π-π Stacking Interactions: Non-Negligible Forces for Stabilizing Porous Supramolecular Frameworks. *Sci. Adv.* **2020**, *6*, eaax9976.
31. Lee, I.-S. H.; Ji, Y. R.; Jeoung, E. H. Reinterpretation of the Brønsted α for Redox Reactions Based on the Effect of Substituents on Hydride Transfer Reaction Rates between $NAD^+$ Analogues. *J. Phys. Chem. A* **2006**, *110*, 3875.
32. Roth, J. P.; Lovell, S.; Mayer, J. M. Intrinsic Barriers for Electron and Hydrogen Atom Transfer Reactions of Biomimetic Iron Complexes. *J. Am. Chem. Soc.* **2000**, *122*, 5486.
33. Marcus, R. A. On the Theory of Oxidation-Reduction Reactions Involving Electron Transfer. I. *J. Chem. Phys.* **1956**, *24*, 966.
34. Grimme, S.; Hansen, A.; Ehlert, S.; Mewes, J.-M. r2SCAN-3c: A "Swiss Army Knife" Composite Electronic-Structure Method. *J. Chem. Phys.* **2021**, *154*.
35. Barone, V.; Cossi, M. Quantum Calculation of Molecular Energies and Energy Gradients in Solution by a Conductor Solvent Model. *J. Phys. Chem. A* **1998**, *102*, 1995.
36. (a) Nelsen, S. F.; Blackstock, S. C.; Kim, Y. Estimation of Inner Shell Marcus Terms for Amino Nitrogen Compounds by Molecular Orbital Calculations. *J. Am. Chem. Soc.* **1987**, *109*, 677; (b) Klimkāns, A.; Larsson, S. Reorganization Energies in Benzene, Naphthalene, and Anthracene. *Chem. Phys.* **1994**, *189*, 25; (c) Auer, B.; Fernandez, L. E.; Hammes-Schiffer, S. Theoretical Analysis of Proton Relays in Electrochemical Proton-Coupled Electron Transfer. *J. Am. Chem. Soc.* **2011**, *133*, 8282.
37. This value for MeCN binding to $Cp^*Ir(bpy)^{2+}$ is calculated at the r2-SCAN-3c level of theory, which was used for calculating the reorganization energy. The different level of theory explains why this MeCN binding energy is different to those presented in Table S6.
38. Ghosh, S.; Horvath, S.; Soudackov, A. V.; Hammes-Schiffer, S. Electrochemical Solvent Reorganization Energies in the Framework of the Polarizable Continuum Model. *J. Chem. Theory Comput.* **2014**, *10*, 2091.
39. (a) Markle, T. F.; Darcy, J. W.; Mayer, J. M. A New Strategy to Efficiently Cleave and Form C–H Bonds Using Proton-Coupled Electron Transfer. *Sci. Adv.* **2018**, *4*, eaat5776; (b) Sayfutyarova, E. R.; Goldsmith, Z. K.; Hammes-Schiffer, S. Theoretical Study of C–H Bond Cleavage via Concerted Proton-Coupled Electron Transfer in Fluorenyl-Benzoates. *J. Am. Chem. Soc.* **2018**, *140*, 15641; (c) Darcy, J. W.; Kolmar, S. S.; Mayer, J. M. Transition State Asymmetry in C–H Bond Cleavage by Proton-Coupled Electron Transfer. *J. Am. Chem. Soc.* **2019**, *141*, 10777; (d) Qiu, G.; Knowles, R. R. Rate–Driving Force Relationships in the Multisite Proton-Coupled Electron Transfer Activation of Ketones. *J. Am. Chem. Soc.* **2019**, *141*, 2721; (e) Sayfutyarova, E. R.; Lam, Y.-C.; Hammes-Schiffer, S. Strategies for Enhancing the Rate Constant of C–H Bond Cleavage by Concerted Proton-Coupled Electron Transfer. *J. Am. Chem. Soc.* **2019**, *141*, 15183; (f) Salamone, M.; Galeotti, M.; Romero-Montalvo, E.; van Santen, J. A.; Groff, B. D.; Mayer, J. M.; DiLabio, G. A.; Bietti, M. Bimodal Evans–Polanyi Relationships in Hydrogen Atom Transfer from $C(sp^3)$–H Bonds to the Cumyloxyl Radical. A Combined Time-Resolved Kinetic and Computational Study. *J. Am. Chem. Soc.* **2021**, *143*, 11759.
40. Pu, J.; Ma, S.; Garcia-Viloca, M.; Gao, J.; Truhlar, D. G.; Kohen, A. Nonperfect Synchronization of Reaction Center Rehybridization in the Transition State of the Hydride Transfer Catalyzed by Dihydrofolate Reductase. *J. Am. Chem. Soc.* **2005**, *127*, 14879.
41. Hammes-Schiffer, S. Nuclear–Electronic Orbital Methods: Foundations and Prospects. *J. Chem. Phys.* **2021**, *155*.
42. (a) Heimann, J. E.; Bernskoetter, W. H.; Hazari, N.; Mayer, J. M. Acceleration of $CO_2$ Insertion into Metal Hydrides: Ligand, Lewis Acid, and Solvent Effects on Reaction Kinetics. *Chem. Sci.* **2018**, *8*, 6629; (b) Heimann,

J. E.; Bernskoetter, W. H.; Hazari, N. Understanding the Individual and Combined Effects of Solvent and Lewis Acid on $CO_2$ Insertion into a Metal Hydride. *J. Am. Chem. Soc.* **2019**, *141*, 10520.
43. In reference 20e, we made preliminary fits of hydride transfer reactions from transition metal complexes to organic hydride acceptors using Marcus theory. However, due to incomplete data sets, the fits were poor quality and estimates for reorganization energy varied by 40 kcal $mol^{-1}$.
44. As discussed by Glusac and co-workers in reference 17, for photochemical $CO_2$ reduction even when $\lambda = 0$, the rate of hydride transfer will barely be able to keep up with the solar photon flux. Therefore, for photochemical reactions it is important to increase the rate of hydride transfer reactions as much as possible.
45. Oevering, H.; Paddon-Row, M. N.; Heppener, M.; Oliver, A. M.; Cotsaris, E.; Verhoeven, J. W.; Hush, N. S. Long-Range Photoinduced Through-Bond Electron Transfer and Radiative Recombination via Rigid Nonconjugated Bridges: Distance and Solvent Dependence. *J. Am. Chem. Soc* **1987**, *109*, 3258.
46. (a) Eberson, L.; Shaik, S. S. Electron-Transfer Reactions of Radical Anions: Do They Follow Outer- or Inner-Sphere Mechanisms? *J. Am. Chem. Soc* **1990**, *112*, 4484; (b) Hubig, S. M.; Rathore, R.; Kochi, J. K. Steric Control of Electron Transfer. Changeover from Outer-Sphere to Inner-Sphere Mechanisms in Arene/Quinone Redox Pairs. *J. Am. Chem. Soc.* **1999**, *121*, 617.

## TOC Graphic

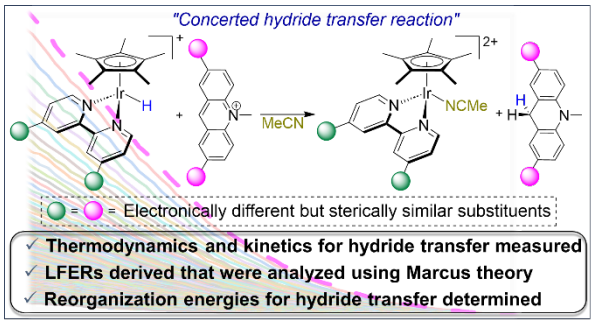
"Concerted hydride transfer reaction"
MeCN
NCMe
= = Electronically different but sterically similar substituents
✓ Thermodynamics and kinetics for hydride transfer measured
✓ LFERs derived that were analyzed using Marcus theory
✓ Reorganization energies for hydride transfer determined